Investigating Immune Checkpoint Inhibitor-Induced Thyroid Dysfunction: Initial Immune Dysregulation Insights and 3D Co-culture Model with Nthy-Ori 3-1 and PBMCs

by

Adeliya Temirbek

A Dissertation Submitted to the
Graduate School of Health Sciences
in Partial Fulfillment of the Requirements for
the Degree of

Master of Science

in

Immunology

August 27, 2024

Investigating ICI-Induced Thyroid Dysfunction: Initial Immune Dysregulation Insights and 3D Co-culture Model with Nthy-Ori 3-1 and PBMCs

Koç University

Graduate School of Health Sciences

This is to certify that I have examined this copy of a master's thesis by

Adeliya Temirbek

and have found that it is complete and satisfactory in all respects,
and that any and all revisions required by the final
examining committee have been made.

Committee Members:

Assoc. Prof Yıldız Tütüncü

Prof. Dr. Savaş Güzel Tekirdağ

Dr. Öğ. Üyesi Hayva Sezer

Date: 27.08.2024

[To the loved ones]

ABSTRACT

Investigating ICI-Induced Thyroid Dysfunction: Initial Immune Dysregulation Insights and 3D Co-culture Model with Nthy-Ori 3-1 and PBMCs

Adeliya Temirbek

Master of Science in Immunology

August 27, 2024

Immune checkpoint inhibitors (ICIs) have revolutionized cancer treatment, significantly improving survival rates across a range of malignancies by reinforcing T cells' ability to recognize and eradicate cancer cells. Despite their effectiveness, ICIs are frequently associated with immune-related adverse events (irAEs), the most prevalent of which is thyroid dysfunction (TD). Rarely, these toxicities may be severe enough to cause therapy to be postponed or terminated. Understanding the mechanisms underlying thyroid irAEs could provide valuable insights into both thyroid autoimmune diseases and the broader spectrum of irAEs linked to ICIs. This study addresses gaps in current research by immunophenotyping patients undergoing ICI therapy at two critical time points: before treatment and three weeks post-treatment. Comparative analyses were performed against control groups of healthy individuals and patients with Hashimoto's thyroiditis. Among the 9 patients studied, 2 developed TD within three weeks of PD-1 inhibitor treatment. Flow cytometry revealed significant increases in IFN-γ producing CTLs and NK cells, along with TNF-α producing B cells and its expression levels in NKT-like cells following the therapy ($p < 0.05$). Notably, the increase in TNF-α producing B cells was more pronounced when compared to all study groups. These findings suggest that immune cell activation and subsequent cytokine production, aimed at combating tumor cells, may also serve as predictive biomarkers for irAEs, including ICI-induced TD. To improve the physiological relevance of in vitro studies, this research also introduces a novel 3D co-culture model using thyroid spheroids derived from the Nthy-ori 3-1 cell line, co-cultured with patient-specific PBMCs. Initial results indicated no significant differences in thyroid cell viability between TD patients and controls in the 3D setting, contrasting with notable viability reductions in 2D co-cultures. Additionally, immunophenotyping performed on 3D co-cultures revealed a substantial increase in B cell populations of the patients on the third week of therapy compared to healthy controls ($p < 0.05$). The findings from both immunophenotyping and in vitro research deepen our understanding of conditions where the pathophysiology is poorly defined, as in the case of ICI-induced TD. Despite limitations related to the allogeneic nature of the approach, this study is pioneering in creating an in vitro model specifically designed to investigate ICI-related irAEs. It offers preliminary insights and establishes a methodological framework for future thyroid research.

Key words: Immune checkpoint inhibitors, immune-related adverse events, thyroid dysfunction, immunophenotyping, 3D co-culture model, Nthy-ori 3-1 cell line, in vitro research, TNF-α, IFN-γ

ÖZETÇE

İmmün Kontrol-noktası İnhibitör Tedavisi Kaynaklı İmmün Disfonksiyonların Araştırılması: Bağışıklık Düzenleme Bozukluklarına Dair İlk Bulgular ve Nthy-Ori 3-1 ile PBMC'lerin Ortak Kültürü

Adeliya Temirbek

İmmünoloji, Yüksek Lisans

Ağustos 27, 2024

İmmün kontrol-noktası inhibitörleri (ICIs), T hücrelerinin kanser hücrelerini tanıma ve yok etme yeteneğini güçlendirerek, çeşitli kanserlere karşın hayatta kalma oranlarını önemli ölçüde artırmış ve kanser tedavisinde devrim yaratmıştır. Ancak, İKİ'lerin etkinliğine rağmen, sıklıkla bağışıklıkla ilişkili yan etki olaylar (irAEs) ile ilişkilendirilirler; bunlar arasında en yaygın olanı tiroid disfonksiyonudur (TD). Nadir durumlarda, bu toksisiteler tedavinin ertelenmesine veya sonlandırılmasına neden olacak kadar şiddetli olabilir. Tiroid irAEs'nin altında yatan mekanizmaların anlaşılması, hem tiroid otoimmün hastalıkları hem de ICIs ile ilişkili irAEs'in daha geniş spektrumu hakkında değerli bilgiler sağlayabilir. Bu çalışma, ICI tedavisi gören hastaların tedavi öncesi ve tedaviden üç hafta sonrası olmak üzere iki kritik zaman noktasında immünofenotiplendirilmesiyle mevcut araştırmalardaki boşlukları ele almaktadır. Sağlıklı bireyler ve Hashimoto tiroiditi olan hastalardan oluşan kontrol gruplarıyla karşılaştırmalı analizler yapılmıştır. İncelenen 9 hastadan 2'si PD-1 inhibitörü tedavisinden üç hafta içinde TD geliştirmiştir. Akış sitometrisi, tedaviyi takiben IFN-γ üreten CTL'ler ve NK hücrelerinde, ayrıca B ve NKT-benzeri hücrelerde TNF-α ekspresyon seviyelerinde önemli artışlar olduğunu ortaya koymuştur ($p< 0.05$). Özellikle, TNF-α üreten B hücrelerindeki artış, tüm çalışma gruplarına kıyasla daha belirgindi. Bu bulgular, tümör hücreleriyle savaşmayı amaçlayan immün hücre aktivasyonu ve bunun sonucunda oluşan sitokin üretiminin, ICI kaynaklı TD'da dahil olmak üzere irAEs için öngören biyobelirteçler olarak da hizmet edebileceğini düşündürmektedir. In-vitro çalışmaların fizyolojik geçerliliğini artırmak için bu araştırma, hastaya özgü PBMC'lerle birlikte Nthy-ori 3-1 hücre hattından türetilen tiroid sferoidlerini kullanarak yeni bir 3D ortak kültür modeli de önermektir. İlk sonuçlar, 3D ortamda TD hastaları ile kontroller arasında tiroid hücresi canlılığı açısından anlamlı bir fark olmadığını, ancak 2D ortak kültürlerde belirgin canlılık azalması gözlemlendi. Ayrıca, 3D ortak kültürlerde sferoidlerde oluşan inflitre hücre immünofenotiplendirmesinde, tedavinin üçüncü haftasında hastaların B hücre popülasyonlarında sağlıklı kontrollere kıyasla önemli bir artış göstermiştir ($p< 0.05$). Hem immünofenotiplendirme hem de in-vitro araştırmalardan elde edilen bulgular, ICI kaynaklı TD vakasında olduğu gibi patofizyolojinin zayıf bir şekilde tanımlandığı durumlar hakkındaki anlayışımızı derinleştirirmeye yardımcı olur . Allojenik yaklaşımın doğasına ilişkin sınırlamalara rağmen, bu çalışma, özellikle ICI ile ilişkili irAEs'i araştırmak için tasarlanmış bir in vitro model oluşturma konusunda öncü niteliktedir. Ön bilgi sunmakta ve gelecekteki tiroid araştırmaları için metodolojik bir çerçeve oluşturmaktadır.

Anahtar Kelimeler: İmmün Kontrol-noktası inhibitörleri, bağışıklıkla ilişkili advers olaylar, tiroid disfonksiyonu, immünofenotiplendirme, 3D ortak kültür modeli, Nthy-ori 3-1 hücre hattı, in vitro araştırma, TNF-α, IFN-γ

AKNOWLEDGEMENTS

First and foremost, I would like to express my deepest gratitude to my supervisor, Dr. Yildiz Tutuncu, for her unwavering support throughout this challenging yet insightful journey. Her guidance and encouragement were invaluable at every stage of my thesis preparation, from developing the hypothesis to refining the final draft. I am truly grateful for her valuable advice and constant belief in my work.

I also want to extend my heartfelt thanks to Dr. Ozgur Albayrak and my dear friend Ceren, whose expertise and assistance were crucial in optimizing the protocols. Their willingness to help and share their knowledge played a significant role in this study.

A special thank you goes to Prof. Krishna from Gutenberg University of Mainz, who kindly invited me to Germany during my study semester to learn advanced 3D techniques. His generosity in providing the Nthy-Ori 3-1 cell line and his support throughout my time in Germany made a lasting impact on my research.

I am particularly grateful to my colleagues in Germany, especially Dr. Rosanna, who supervised me closely and patiently taught me all the methodologies I needed to master. Her mentorship was invaluable, and I am deeply appreciative of her guidance.

My sincere thanks go to my group mates, Sana and Amir, who supported me and helped whenever I needed it, without a moment's hesitation. Their friendship and encouragement made even the toughest moments easier to bear.

Finally, I want to extend my deepest appreciation to my family. Your unwavering support through the hardest moments of my life gave me the strength and determination to complete this thesis. I couldn’t have done it without you. Thank you from the bottom of my heart.

TABLE OF CONTENTS

LIST OF TABLES

LIST OF FIGURES

ABBREVIATIONS

APCs Antigen-Presenting Cells

CD Cluster of Differentiation

CFSE Carboxyfluorescein Succinimidyl Ester

CTLs Cytotoxic T Lymphocytes

CTLA-4 Cytotoxic T-Lymphocyte-Associated Protein 4

DCs Dendritic Cells

DMSO Dimethyl Sulfoxide

FACS Fluorescence-Activated Cell Sorting

FBS Fetal Bovine Serum

fT3 Free Triiodothyronine

fT4 Free Thyroxine

FSC-A Forward Scatter Area

FSC-H Forward Scatter Height

HT Hashimoto's Thyroiditis

ICIs Immune Checkpoint Inhibitors

IFN-γ Interferon-Gamma

IL Interleukin

IRB Institutional Review Board

irAEs Immune-Related Adverse Events

LAG-3 Lymphocyte-Activation Gene 3

MFI Mean Fluorescence Intensity

MHC Major Histocompatibility Complex

MTT 3-(4,5-Dimethylthiazol-2-yl)-2,5-Diphenyltetrazolium Bromide

NIS Sodium/Iodide Symporter

NK Natural Killer Cells

NKT-like Cells Natural Killer T-like Cells

PBMCs Peripheral Blood Mononuclear Cells

PD-1 Programmed Death-1

PD-L1 Programmed Death-Ligand 1

PMA Phorbol 12-Myristate 13-Acetate

PBS Phosphate-Buffered Saline

RPMI Roswell Park Memorial Institute Medium

SCC Squamous Cell Carcinoma

SSC-A Side Scatter Area

TD Thyroid Dysfunction

Th T Helper Cells

TNF-α Tumor Necrosis Factor-Alpha

TCR T Cell Receptor

Tregs Regulatory T Cells

TSH Thyroid-Stimulating Hormone

Chapter 1: **INTRODUCTION**

Immune checkpoint inhibitors (ICIs) have markedly increased survival rates for cancer patients and have become the first-line treatment for several types of tumors. Cancer cells utilize multiple strategies to elude the immune system, a phenomenon referred to as immune evasion, which plays a critical role in the advancement and dissemination of tumors. The mechanisms involved in this process consist of the impairment of antigen presentation, the release of immunosuppressive cytokines, the attraction of regulatory T cells (Tregs), and the overexpression of immune checkpoint proteins [Dutta et al., 2023]. ICIs are a revolutionary category of cancer therapies that boost the immune system's ability to fight against malignancies. This is accomplished by focusing on particular proteins that typically serve as "brakes" on immune responses. By inhibiting these checkpoints, ICIs enhance the ability of T cells to identify and eliminate cancer cells [Pardoll, 2012].

However, the vast potential of checkpoint inhibitors is hindered by a range of inflammatory toxicities known as immune-related adverse events (irAEs), which have hampered their widespread use. Dermatitis, colitis, and thyroiditis are some of the most frequently observed irAEs. However, the mortality rate is particularly high for the more uncommon conditions, such as myocarditis, myositis, and encephalitis. Remarkably, after initiating ICI therapy, up to 85% of patients treated with anti-PD-1 (Programmed Death-1) and 95% of patients receiving combined CTLA-4 (cytotoxic T-lymphocyte-associated protein) and PD-1 blocking have adverse reactions of any kind [Hommes et al., 2021]. In rare circumstances, these toxicities may be life-threatening and result in treatment delays or discontinuations. Unlike the negative effects caused by chemotherapy and targeted therapy, irAEs are challenging to anticipate due to their unpredictable severity and timing [Wang et al., 2023]. While most irAEs often occur within a few weeks of initiating ICI therapy, there have been cases where the manifestation occurred years after treatment initiation, and the precise onset time remains uncertain [Chye et al., 2022].

Notably, thyroid dysfunction (TD) stands out as the most prevalent irAEs associated with ICI immunotherapy. Based on recent systematic reviews and meta-analyses, the occurrence of TD is influenced by the specific class of ICIs employed. Approximately 7% of patients undergoing anti-CTLA-4 therapy, 19% of those PD-1 and Programmed Death-Ligand 1 (PD-L1) inhibitors, and 28% of patients treated with combination therapies experience TD of various types. On top of that, TDs were implicated in as much as 50% of patients receiving combination therapy, according to recent studies [Stelmachowska-Banaś and Czajka-Oraniec 2020]. In alignment with the incidence rates observed in the general population, TDs are more prevalent among younger patients and women. Additionally, there is no statistically significant correlation between the occurrence of TD and the dosage of ICIs or the specific type of tumor being treated [Karaviti et al., 2024]. Complicating factors for the thyroid during the therapy include preexisting autoimmune diseases, the presence of anti-thyroid antibodies, high BMI levels and elevated 18FDG uptake in the thyroid prior to treatment [Yamauchi et al., 2019].

TD encompasses various clinical presentations, such as thyroiditis, hypo- and hyperthyroidism, and Graves' disease. A common manifestation is a type of destructive thyroiditis that is characterized by a brief period of mild to moderate thyrotoxicosis [Karaviti et al., 2024]. This is frequently followed by a return to normal thyroid function or, within one to three months of starting ICI therapy, a progression into overt hypothyroidism, which can be defined by variable levels of increased Thyroid-Stimulating Hormone (TSH) levels [Illouz et al., 2017]. Management of ICI-induced TD typically involves regular monitoring of thyroid function tests and symptomatic treatment. Laboratory testing including TSH, free triiodothyronine (T3) and free thyroxine (T4) are considered important for pre- and post-ICI therapy check-ups [Deligiorgi et al., 2021]. Particularly, measurement of these hormones is recommended prior to each treatment cycle. Unlike other irAEs, endocrine problems including TD may require long-term hormone replacement therapy and reveal limited response to immunosuppressive drugs such corticosteroids [Nervo et al., 2023]. Remarkably, the occurrence of TD has been linked to improved treatment results and higher rates of survival. This contradictory phenomenon indicates that the immunological activation responsible for TD or any other irAEs may also reinforce the body's capacity to combat

tumors. Further investigation is required to comprehend these mechanisms and ascertain whether the emergence of such complications can function as a prognostic indicator for positive results in patients [de Filette et al., 2022].

Despite extensive research on ICI-related TD, the exact mechanisms behind this disorder are still unknown. The pathophysiology of thyroid irAEs is thought to entail the development of destructive thyroiditis caused by an acute autoimmune response driven by T cells [Karaviti et al., 2024]. Recently, TD has been associated with inflammatory markers, including cytokines, TNF-α and IFN-γ, which cause tissue injury by recruiting, activating, and invading inflammatory cells into the thyroid. This chronic inflammation not only directly damages the thyroid cells but also induces the production of autoantibodies that target thyroid antigens, thereby exacerbating TD [Chera et al., 2022]. Nevertheless, given the thyroid gland's heightened susceptibility to autoimmune attacks and the possible involvement of endocrine-specific autoantibodies in irAEs, it is postulated that a breakdown in immune tolerance to autoantigens, resembling the processes observed in autoimmune thyroid disorders, may play a significant role in the development of this dysfunction [Wang et al., 2023]. Hence, elucidating the mechanisms behind thyroid irAEs could offer insights into not only thyroid autoimmune diseases but also other irAEs [Iwama et al., 2022].

ICI-induced irAEs poses substantial hurdles for both academics and physicians due to its varied onset and poorly characterized mechanism. Immunophenotyping studies have played an essential part in understanding the underlying mechanisms of these conditions by providing detailed information about the roles and characteristics of certain types of immune cells. Flow cytometry in this case is advantageous for quickly examining various cell populations. This method provides extensive information on cell size, complexity, and phenotype [Tembhare et al., 2022]. In order to uncover predictive biomarkers and potential disease-causing pathways, this strategy can shed light on changes in immune cell composition and inflammatory levels that take place during each cycle of ICI treatment. The scarcity of immunophenotyping studies in this subject, in spite of its importance, emphasizes the urgent need for more thorough investigation.

Furthermore, novel in-vitro approaches that yield reproducible outcomes and are characterized by precisely controlled conditions are fundamentally required to progress beyond improving research on immunophenotyping of patient samples. When applied to ICI-induced TD, these methods can be helpful in analyzing the cellular and molecular processes. Utilizing sophisticated 3D culture models, such as thyroid spheroids, can offer significant advantages in terms of enhancing the physiological accuracy. The incorporation of peripheral blood mononuclear cells (PBMCs) that are distinct to each patient may add more of a patient-specific approach [Edmondson et al., 2014]. By examining the behavior and composition of PBMCs derived from various patient groups in the presence of thyroid spheroids, scientists might detect certain patterns that may contribute to a better understanding of the underlying mechanisms. Moreover, the research on other thyroid autoimmune disorders may potentially benefit from this refined study approach. Technically optimizing such novel in-vitro models is a critical first step toward tailored treatment strategies, and ICI-induced TD provides a compelling case study for this purpose.

Chapter 2: **BACKGROUND INFORMATION AND OBJECTIVES**

2.1 Immune Checkpoint Inhibitors

The 2018 Nobel Prize in Physiology or Medicine was awarded to ICIs, which introduced a revolutionary approach to the treatment of numerous malignancies. This discovery significantly improved the survival rates of patients with melanoma and lung cancer, with survival rates raising from 4% with conventional treatments to as high as 50% with ICIs [Dobosz and Dzieciątkowski, 2019]. The first licensed ICI by the Food and Drug Administration (FDA) in 2011, ipilimumab, selectively targets CTLA-4 to enhance T-cell-mediated antitumor response and significantly extend the survival of metastatic melanoma patients. In 2014, the FDA approved nivolumab, the first PD-1 inhibitor, specifically for the treatment of metastatic melanoma. Nivolumab has been shown to improve overall survival and maintain tumor remission following treatment. Accordingly, the FDA has approved a number of monoclonal antibodies that block PD-1 or its ligand, PD-L1. Melanoma, lung cancer, lymphoma, esophageal carcinoma, gastric cancer, and hepatocellular carcinoma are just a few of the cancer types for which these antibodies have been approved for application, either standalone or in conjunction with other therapy [Meng et al., 2024]. More recently, in addition to CTLA-4 and PD-1/PD-L1 inhibitors, a new class of ICIs targeting LAG-3 (Lymphocyte-Activation Gene 3) has been developed. In 2022, the FDA approved the first LAG-3 inhibitor, relatlimab, which is combined with nivolumab under the brand name Opdualag in treating unresectable or metastatic melanoma. Thereby, currently, the key FDA-approved ICIs include ipilimumab (Yervoy) for CTLA-4 inhibition; pembrolizumab (Keytruda), nivolumab (Opdivo), and cemiplimab (Libtayo) for PD-1 inhibition; atezolizumab (Tecentriq), durvalumab (Imfinzi), and avelumab (Bavencio) for PD-L1 inhibition; and the newly approved relatlimab (Opdulag), targeting the LAG-3 pathway With the expanding range of tumor types that have shown clinical effectiveness with ICIs, it is anticipated that its application would rise in the future [Twomey and Zhang, 2021; Su et al., 2023].

Table 2.1: Immune checkpoint inhibitors, cancer types, and efficacy defined by the overall response rate which is the percentage of patients whose tumors considerably shrink or vanish after treatment

Name	Inhibitor Type	Cancer Type	Overall Response Rate	Reference
Ipilimumab	CTLA-4 Inhibitor	Metastatic melanoma	Overall response rate 10.9%	[Evan et al., 2010]
Nivolumab	PD-1 Inhibitor	Advanced melanoma	31.7% in previously treated patients	[Weber et al., 2015]
		Non-Small Cell Lung Cancer	20% in patients with squamous-cell NSCLC	[Brahmer et al., 2015]
Pembrolizumab	PD-1 Inhibitor	Advanced melanoma	33% in previously untreated patients	[Robert et al., 2019]
		Non-Small Cell Lung Cancer	45% in patients with PD-L1 expression ≥50%	[Reck et al., 2016]
Cemiplimab	PD-1 Inhibitor	Cutaneous squamous cell carcinoma	Overall response rate 47.2%	[Migden,2018]
Durvalumab	PD-L1 Inhibitor	Non-Small Cell Lung Cancer	16% in patients with stage III Non-Small Cell Lung Cancer	[Antonia et al., 2017]
		Urothelial carcinoma	17.8% in patients with	[Powles et al., 2020]

			untreated urothelial carcinoma	
Atezolizumab	PD-L1 Inhibitor	Non-Small Cell Lung Cancer	14% in patients with previously treated Non-Small Cell Lung Cancer	[Rittmeyer et al., 2017]
		Urothelial carcinoma	23% in patients with advanced urothelial carcinoma	[Powles et al., 2018]
Avelumab	PD-L1 Inhibitor	Merkel cell carcinoma	Overall response rate 33%.	[Kaufman et al., 2016]
		Urothelial carcinoma	16.1% in patients with advanced urothelial carcinoma	[Powles et al., 2020]
Relatlimab in combination with nivolumab	LAG3 Inhibitor	Unresectable or Metastatic Melanoma	Overall response rate 43.1%	[Akkooi, 2024]

2.2 Immune Checkpoint Inhibitors' Mechanisms of Action

Immune surveillance integrating both the innate and adaptive immune systems checks and regulates the tumor's microenvironment. In this surveillance, antigen-presenting cells (APCs) play a critical role by identifying and presenting tumor neoantigens to naive T-cells, serving as a bridge between innate and adaptive immunity. T cell activation occurs when naive T cells interact with Major Histocompatibility Complex (MHC) molecules on APCs. The T cell receptor (TCR) recognizes and binds to the tumour neoantigen displayed by the MHC on the APC. This interaction, along

with co-stimulatory signals such as CD28 binding to B7 ligands, triggers T cell activation and initiates an immune response against the tumor. Nevertheless, cancer cells employ many tactics to evade the immune system, such as compromising antigen presentation and overexpression of immune checkpoint proteins [Dutta et al., 2023]. The immune checkpoints that have been widely investigated, PD-1 and CTLA-4, interact with their respective ligands, which are present on the surface of APCs or tumor cells (PD-L1/2 and CD80/86). Thus, the purpose of ICIs is to prevent the establishment of inhibitory signals through these interactions [Alturki, 2023].

(a)

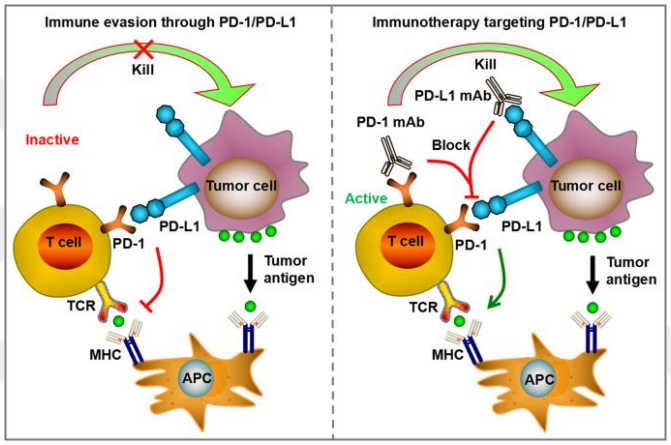

(b)

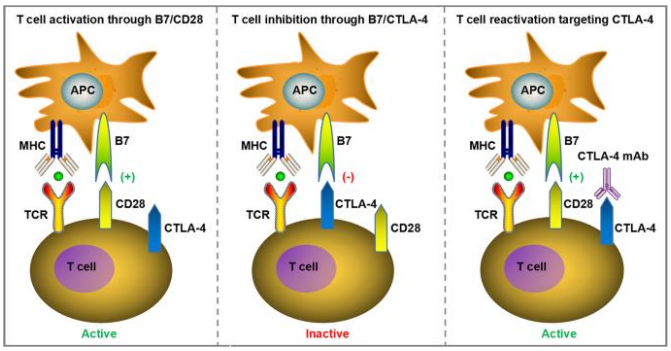

Figure 2.1: An overview of Immune Checkpoint Inhibitors' mechanisms of action with (a) and (b) corresponding to PD-1/PD-L1 and CTLA-4, respectively. Extracted from [Meng et al., 2024].

2.2.1 PD-1/PD-L1

The PD-1/PD-L1 pathway is one of the most extensively studied immune checkpoint mechanisms and plays a crucial role in clinical cancer therapies. PD-1, also

known as CD279, is a type I transmembrane glycoprotein belonging to the CD28 superfamily, characterized by an immunoglobulin variable domain, a transmembrane segment, and a cytoplasmic region containing immunoreceptor tyrosine-based inhibitory motif (ITIM) and immunoreceptor tyrosine-based switch motif (ITSM). Predominantly expressed on activated T cells, PD-1 can also be found on B cells, NK cells, monocytes, dendritic cells (DCs), myeloid cells, and neutrophils. PD-L1, often referred to as CD274 or B7-H1, serves as the primary ligand for PD-1. It is part of the B7 family and is present on a variety of immune cells, including T cells, B cells, DCs, macrophages, and mast cells. Additionally, PD-L1 is expressed by normal tissue cells such as hepatocytes, pancreatic islet cells, endothelial cells, thyroid cells, as well as various tumor cells [Paschou et al., 2021]. The interaction between PD-1 and PD-L1 leads to the phosphorylation of PD-1's cytoplasmic ITIM and ITSM, resulting in the inhibition of TCR signaling. Anti-PD-1 and anti-PD-L1 antibodies disrupt this interaction, thereby enhancing the immune system's capacity to eliminate cancer cells and restoring T cell function [Kim et al., 2022; Patsoukis et al., 2020].

2.2.2 CTLA-4

CTLA-4, or CD152, is a cell membrane receptor that interacts with the same B7 ligand as the co-stimulatory receptor CD28. CTLA-4 is exclusively found on activated T cells and is mostly observed on the surface of immunosuppressive Tregs. CTLA-4 and CD28 bind to the B7 ligands CD80 (B7-1) and CD86 (B7-2) presented on APCs as a result of their comparable structural similarity. CTLA-4 exhibits a greater binding strength to its ligand in comparison to CD28, therefore delivering a suppressive signal to the T cell. This signal decreases the synthesis of IL-2, a crucial cytokine for T cells, halts the progression of the cell cycle, and hinders the expansion of T cells. In addition, CTLA-4 attracts phosphatases to its internal domain, which remove phosphate groups from signaling molecules located downstream of the TCR and CD28. This process further reduces the activation of T cells. Moreover, it was found that CTLA-4 inhibits the role of CD28 in the process of T cell activation by either removing or decreasing the expression of CD80 and CD86 on APCs. Blocking CTLA-4 with a monoclonal antibody prevents its interaction with CD80/CD86. The inhibition of CTLA-4 removes the inhibitory restriction, enabling CD28 to attach to these ligands and deliver the

essential co-stimulatory signals for T cell activation [Lingel and Brunner-Weinzierl, 2019; Hosseini et al., 2020].

2.3 Thyroid Dysfunction Following Immune Checkpoint Inhibitor Therapy

The thyroid gland is particularly susceptible to the immune-related effects of ICIs, which can result in conditions such as destructive thyroiditis, hypothyroidism, or in rare cases, Graves' disease. Important indicators of the development of ICI-induced TD include alterations in thyroid hormone levels, particularly those in TSH, fT3, and fT4. Monitoring these hormone levels can assist in the identification of suitable management strategies that are tailored to the specificity of the thyroid disorder exhibited by the patient [Karaviti et al., 2024].

2.3.1 Destructive Thyroiditis

An inflammatory disorder of the thyroid gland that results in the destruction of thyroid tissue is known as destructive thyroiditis. According to a study by [Lu et al., 2022], 9.3% of patients receiving ICIs experienced destructive thyroiditis, with hyperthyroidism usually developing on before hypothyroidism. Typically, this thyroiditis progresses through a 4 to 6 weeks of thyrotoxicosis phase, during which thyroid tissue is destroyed and stored thyroid hormones are released, resulting in symptoms including anxiety, tremors, and weight loss. This phase is followed by hypothyroidism. Subclinical thyrotoxicosis is described as suppressed TSH with normal fT4 and TT3 serum levels, whereas overt thyrotoxicosis is characterized by high fT4 and suppressed TSH serum levels [de Filette et al., 2016]. Broad thyroid gland enlargement, reduced internal blood flow, and decreased internal echogenicity are characteristic ultrasonic markers of ICI-induced destructive thyroiditis. Among patients receiving combination therapy with anti-PD-1 and anti-CTLA-4 inhibitors, the incidence of hypothyroidism associated with this disorder is particularly high, up to 66% [Cardona et al., 2023]. During the hyperthyroid phase of the destructive thyroiditis, beta-blockers are used to manage tachycardia and anxiety. Corticosteroids may be used to reduce inflammation in extreme cases. Levothyroxine is prescribed as thyroid hormone replacement treatment once the hypothyroid phase has developed with dosage adjustments based on routine thyroid function testing [Iyer et al., 2018].

2.3.2 Hypothyroidism

An underactive thyroid gland that produces insufficient thyroid hormones—which are vital for controlling metabolism, energy production, and other bodily functions—defines hypothyroidism. The immune system damaging the thyroid cells during a destructive thyroiditis process is often followed by the hypothyroid phase. In many cases, this damage is unrecoverable and results in persistent hypothyroidism [Kassi et al., 2019]. As per the latest findings, around 3.9-8.5% of patients receiving anti-PD-1, 3.9-8.5% receiving anti-PD-L1 therapy, and 2.5-5.2% of patients receiving CTLA-4 inhibitors are associated with hypothyroidism. With an incidence varying from 10.2 to 16.4%, combination therapy with ICIs can lead to higher rates [Karaviti et al., 2024]. Primary hypothyroidism is diagnosed by elevated TSH along with low or low-to-normal fT4. On the other hand, low or abnormally low-to-mid-normal TSH levels together with low fT4 are indicative of secondary or central hypothyroidism, which is linked to pituitary disorders such hypophysitis. When fT4 is normal and TSH increased but less than 10 mIU/mL, subclinical hypothyroidism can be diagnosed [de Filette et al., 2016].

2.3.3 Graves' Disease

Graves' disease (GD) is an autoimmune condition characterized by hyperthyroidism, which is a condition in which the TSH receptor is activated by autoantibodies, producing an excessive amount of thyroid hormones. Patients on ICI therapy have a hyperthyroidism incidence that includes GD varying between 0.2 to 1.7% for CTLA-4 inhibitors, 0.6 to 3.7% for PD-1/PD-L1 inhibitors, and 8 to 11% for combination therapies [Chera et al., 2022]. The activation of the immune system by ICIs is a crucial factor in the pathogenesis of GD, which is likely to trigger an autoimmune response in individuals who are genetically predisposed. High levels of T4 and T3, noticeable early symptoms, the persistence of thyrotoxic manifestations for more than six weeks, and the presence of other hallmark indicators, such as orbitopathy or a big goiter, increase the suspicion of Graves' disease. Using antithyroid medications, such as methimazole or propylthiouracil, to reduce thyroid hormone production is part of GD managing. Individuals who experience severe or ongoing hyperthyroidism may benefit from thyroidectomy or radioactive iodine treatment [Wiersinga, 2019]. Studies show that whereas 30–40% of patients may only experience one episode of hyperthyroidism,

60–70% of Graves' disease cases proceed over an extended period of time with recurring episodes [Deligiorgi et al., 2021].

2.4 Pathophysiology of ICI-induced Thyroid Dysfunction & Relation to Autoimmunity

Generally, upon entering the tumor microenvironment, activated T cells experience up-regulation of PD-1/CTLA-4 molecules, which then bind to PD-L1/PD-L2 or CD80/CD86 molecules on tumor cells. As a result, the immune system is unable to detect and destroy tumor cells, and the microenvironment becomes immunosuppressive, allowing tumor cells to proliferate uncontrollably. It is believed, that toxicities associated with ICIs which block these interactions can develop when activated T cells destroy tumor cells while simultaneously attacking healthy human tissue cells (Figure 2.2).

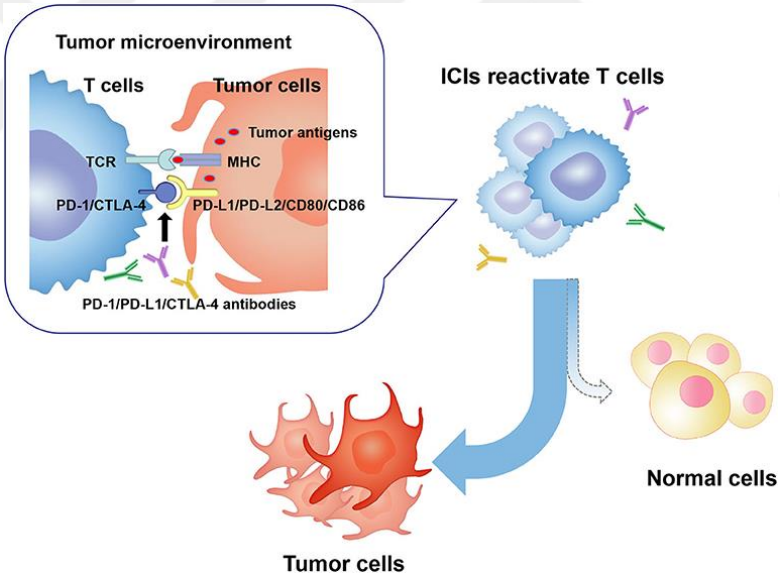

Figure 2.2: An overview of ICI-induced irAEs. Extracted from [Xu et al., 2020].

Moreover, it has been demonstrated that the ability of a TCR to bind multiple peptides is of significant importance in autoimmune responses. Due to the structural similarity between peptide-loaded MHCs that appear to be unrelated, peptides might activate autoreactive T cells. Similar shared antigen recognition in tumor and affected organs in the development of irAEs and tumor-derived T cell infiltration into healthy tissues, as well as identical TCR sequences in both tumor and healthy tissue, are all documented in studies [Taylor et al., 2022]. Treatment with anti-CTLA-4 was

demonstrated to expand the peripheral TCR repertoire in melanoma patients, with a difference between those who experienced irAEs and those who did not. It was discovered that administering an anti-CTLA-4 monoclonal antibody led to an increase in the amount of distinct T-cell receptor beta-chain (TCR V-β) sequences that were produced through genetic recombination. The alterations in T cell populations occurred early upon treatment, indicating a potential correlation with the eventual emergence of irAEs. Although there may be initial alterations, toxicity typically arises at a later stage in treatment, suggesting that pathogenic T cells may progressively develop from the greater pool of clonotypes following checkpoint blocking [Robert et al., 2014].

Additionally, irAEs may be the result of the off-target effects of ICIs on non-hematopoietic cells that express the intended immune checkpoint. Anti-CTLA-4 antibodies have a higher tendency to specifically affect the pituitary gland, but anti-PD-1 antibodies are frequently linked to the occurrence of TDs. This connection pertains to the expression of CTLA-4 in the pituitary gland, specifically on cells responsible for the secretion of prolactin or TSH. Furthermore, recent research by [Deligiannis et al., 2021] has discovered the presence of PD-L1 and PD-L2 in normal thyroid tissue, as evidenced by both mRNA and protein levels. According to [Iwama et al., 2014], the injection of a monoclonal antibody directly binds to the thyroid cell, causing anti-PD1/PD-L1-induced thyroid toxicity. It appears that the interaction between PD-1-expressing lymphocytes and PD-L-expressing thyrocytes may play a role in preventing autoimmune damage to the thyroid tissue.

Although it is obviously clinically important to comprehend the molecular and cellular mechanisms underlying irAEs, these toxicities also provide insight into the fundamental mechanisms governing human immune control. IrAEs are the "phenotype" of loss of function caused by the targeted receptors. This shed light on the pathways and cells that CTLA-4 and PD-1/PD-L1 regulate in the "steady state" and how a breakdown in that regulation results in disease. There are a number of ICI toxicities that resemble well-known autoimmune disorders, however it's unclear if these conditions actually share the same signs [Wang et al., 2023]. This is most evident in endocrine toxicities, such as ICI-induced TD, which bears a striking resemblance to Hashimoto's thyroiditis (HT). Similar to HT, studies have revealed intrathyroidal T lymphocyte increase in the

thyroid tissues of ICI-thyroiditis patients. As opposed to years as in the case of HT, the thyroid gland degeneration in ICI-thyroiditis happens more quickly—over the course of weeks. In addition, the characteristic anti-thyroid antibodies seen in HT are absent in roughly half of the patients with ICI-thyroiditis. These variations imply that although ICI-thyroiditis and HT may share certain pathways, they are also caused by different immunological processes [Lechner et al., 2023].

2.5 Inflammation and The Role of Pro-inflammatory Cytokines

Immune cell activation after ICI therapy can lead to increased production of pro-inflammatory cytokines such as tumor necrosis factor-alpha (TNF-α) and interferon-gamma (IFN-γ), causing systemic inflammation and tissue damage. [Taylor et al., 2023] has suggested that this release has the capacity to induce autoimmune responses by inflicting damage on tissues in close contact with the tumor. Furthermore, there is a hypothesis that proposes that the underlying mechanisms of ICI-induced TD might be an exclusively inflammatory based destructive processes that is distinct from typical autoimmunity mechanisms [Lee et al., 2023]. Overall, there is a lack of information addressing the roles of pro-inflammatory cytokines in ICI-induced thyroiditis. With a relatively limited understanding of the mechanisms involved, various theories exist that require further investigation.

2.5.1 IFN-γ and TNF-α

TNF-α and IFN-γ, generated by inflammatory cells, perform crucial functions in the immune system and tumor surveillance. It has been revealed that these cytokines efficiently induce cell death and exert potent anti-cancer actions by activating several signaling pathways including nuclear factor-κB (NF-κB), mitogen-activated protein kinase (MAPK), and JAK/STAT [Shen et al., 2018]. The elevated levels of these cytokines have been investigated as potential prognostic markers in ICI therapy, and they are occasionally associated with enhanced clinical outcomes. Their increased levels, however, may potentially be a factor in irAEs since an overactive immune system can cause tissue damage to non-tumor tissues. It is possible that irAE is a form of secondary damage, as high expression can lead to exacerbation of inflammation [Hu et al., 2023].

When it comes to ICI-induced TD, the levels of these cytokines were observed to be elevated, although the precise functions and relationships are still being investigated. According to several pathways are involved in the development of thyroid abnormalities as a result of IFN's administration. On thyroid epithelial cells, it can cause the ectopic production of MHC class II molecules, which are typically present on DCs, macrophages, and B lymphocytes. It is believed that this expression elevates the presentation of thyroid antigens to autoreactive lymphocytes [Chalan et al., 2018]. Due to the conflicting findings regarding whether TNF-α is a positive or negative biomarker in ICI patients, the role of TNF-α remains less understood [Kim et al., 2022]. Detailed information regarding the functions of these cytokines as predictive biomarkers and their potential involvement in ICI-induced irAE may be obtained by elucidating the patterns of their expression during the course of ICI therapy.

2.6 Dysregulation in Immune Cell Populations Following ICI Therapy

The complex relationship between immune cells and irAE following ICI therapy is clearly established. Various findings regarding the alteration in immune cell composition are reported. These patterns are being defined and correlated through ongoing research to broaden our understanding of the intricate mechanisms involved.

2.6.1 T cells

As a diverse and crucial subset of lymphocytes, T cells develop and go through positive and negative selection in the thymus. The TCR and the pan-T-cell co-receptor CD3 are present on all T lymphocytes. The ability to identify MHC I or MHC II on APCs is determined by the co-receptor – CD4 or CD8. The main types of T cells are CD8+ T lymphocytes (CTLs), CD4+ T lymphocytes (Helper T cells or Th or THLs), and Tregs, which have CD4 and CD25 bound as co-receptors to their TCRs. T cells largely contribute to the development of organ and tissue autoimmunity via the following mechanisms: activated T cells proliferate and differentiate, eventually becoming effector T cells, and release a variety of inflammatory factors. Furthermore, tissue injury causes an increase in the exposure of tissue self-antigen, which in turn stimulates the activation of additional T cells in a positive feedback cycle. As a result,

the self-immune response will be eradicated by activating Tregs, immunological checkpoint molecules, and other inhibitory pathways [Zhan et al., 2021].

Within the framework of ICI-induced TD, which is recognized as a T cell-mediated mechanism, CD8+ T cells play a critical role by directly causing harm to thyroid cells. The cytotoxic action directly contributes to the development of thyroiditis and eventual hypothyroidism [Lechner et al., 2023; Voskoboinik et al., 2015]. CD4+ T cells, namely the Th1 subset, release pro-inflammatory cytokines such as IFN-γ, IL-2, and TNF-α upon activation by ICIs. The presence of these cytokines intensifies the inflammatory environment within the thyroid, leading to the recruitment and activation of more inflammatory cells [Chera et al., 2022].

Tregs, which are generally responsible for maintaining immunological tolerance and preventing autoimmunity, are also impacted by ICI therapy. ICIs disturb the balance of Tregs, diminishing their inhibitory capacity and enabling heightened activation of autoreactive T cells. CTLA-4 inhibition was demonstrated to hinder the function and survival of Treg cells, resulting in an increased ratio of effector T cells to Treg cells. This imbalance has been found to disrupt peripheral tolerance, potentially leading to the onset of autoimmune conditions in different types of cancer [González-Navajas et al., 2021].

2.6.2 B cells

B cells play a vital role in the adaptive immune system and can be distinguished by the presence of the CD19 surface marker, among others. CD19, a pan-B cell marker, is expressed throughout the whole process of B cell development, from its initiation to the differentiation into plasma cells. The main functions of B cells include secreting cytokines, presenting antigens, and producing antibodies — all of which are critical for mounting an adequate immune response. Through their differentiation into plasma cells, B cells acquire the ability to produce antibodies that specifically target antigens, thereby aiding in the infections' neutralization and removal. Among the cytokines released by B cells and implicated in immune modulation are TNF-α, IL-6, and IL-10 [Althwaiqeb et and Bordoni, 2023].

In patients with previously existing autoimmune disorders characterized by autoantibody generation, the role of B cells in irAEs in particular significant. Even though the exact effects on autoantibody production are not established, ICIs may further exacerbate such disorders. Changes in B cell populations, such as a reduction in circulating B cells, have been observed in patients who have been treated with ICIs. The exact role of B lymphocytes in the anti-tumor response and the emergence of irAEs need additional research [Singh et al., 2023].

2.6.3 NK and NKT-like Cells

NK cells, which are big granular lymphocytes devoid of the common T cell markers CD3 and the human TCR, are identified by the expression of CD56 and CD16. Numerous immunoreceptors can be found on the surface of NK cells, and these receptors can either activate or inhibit the cells' ability to function. Inhibitory receptors, which are present on the majority of nucleated cells, are composed of cytoplasmic ITIM and function to identify MHC I molecules. On the other hand, by recognizing the ligands expressed by damaged cells, activating receptors interact with cell signaling pathways to initiate effector activities. Pro-inflammatory cytokines and chemokines are produced and released by NK cells in order to attract additional immune effector cells to the target region [Rahman and Bordoni, 2023]. In the case of ICI-induced thyroiditis, the number of NK cells was shown to be higher under anti-PD-1 treatment, suggesting a potential involvement in the pro-inflammatory processes [Illouz et al., 2023].

NKT-like cells are defined as CD56+ CD3+ T cells, which have been recognized as a distinct subset of T cells, and demonstrate the greatest ability to destroy cancer cells. While the impact of NKT-like cells on ICI's irAEs is yet to be investigated, it is known that these cells are potent suppliers of IFN-γ and TNF-α. It is anticipated that NKT-like cells, when their effector activity is dysregulated, contribute to the elevated cytokine milieu characteristic of inflammation and may further contribute to the development of irAEs or, in particular, TDs [Almeida et al., 2023].

2.7 Improving Thyroid Dysfunction Studies Through Immunophenotyping and Advanced In-vitro Models

Despite progress in comprehending ICI-induced TD, there is a significant lack of literature and an incomplete understanding of the underlying immune mechanisms, which has resulted in the unexploration of numerous research areas. The pathophysiology of this condition has been enriched through immunophenotyping studies, which have elucidated the specific types and functions of immune cells. CD or Clusters of Differentiation, which were frequently referenced, are specific molecules that are present on the surface of cells and function as markers to differentiate between various cell types [Abbas, 2017]. Immunophenotyping is a method that employs flow cytometry and other techniques to evaluate the expression of intracellular molecules and surface markers in immune cells. Flow cytometry, in particular, facilitates the rapid analysis of a wide range of cell populations, generating detailed data on cell size, complexity, and phenotype by passing fluid-immersed cells through a laser beam at a rate of thousands of cells per second [Tembhare et al., 2022]. There are numerous reasons why it is essential to perform immunophenotyping during each cycle of ICI therapy. First of all, the identification of patients who are at a higher risk of developing irAEs can be facilitated by comprehending the specific changes in immune cell populations. Secondly, the mechanisms that underlie both the therapeutic effects and adverse reactions can be elucidated by monitoring immune cell dynamics. Finally, detailed immunophenotyping can identify biomarkers that can be used to predict responses to ICI therapy [Karaviti et al., 2024].

The main results of immunophenotyping investigations have consistently demonstrated that patients with thyroid irAEs have an increased activity and proliferation of CTLs and Th1. Pro-inflammatory responses were observed to be predominant, with Th1 cells being the primary source of elevated levels of cytokines such as TNF-α, IL-6, and IL-17 [Chera et al., 2022]. The studies reported an increase in CD4+ and CD8+ T cells, as well as NK cells. Furthermore, Tregs were found to have suppressive activity and decreased frequency [Romano et al., 2015]. However, these findings are not consistently supported and vary across blood and thyroid immunophenotyping. Hence, the immunophenotyping of patients with irAEs is

significantly incomplete, and contradictory. The precise function of autoantibodies is still uncertain, and there is no agreement on whether it is primarily caused by autoimmunity or cytotoxicity [Olsson-Brown et al., 2020]. On top of that, the biochemical and clinical variations of TD over time in these patients are poorly documented [Jordan et al., 2023]. To effectively define patterns of ICI-induced TD and other irAEs, as well as their correlations with conditions such as autoimmunity, it is crucial to thoroughly analyze clinical data and investigate immune alterations that occur throughout each stage of ICI therapy. This approach will help in identifying predictive biomarkers and deepening our understanding of the underlying mechanisms.

It is essential to implement cost-effective and consistent methodologies and study models in addition to immunophenotyping studies. The research employs both in vitro and in vivo models, each of which has its own unique advantages and limitations (Figure 2.3). In vivo models, particularly animal models, are a significant asset to immunology research due to their capacity to replicate intricate immunological interactions in a living organism. For instance, a mouse model investigation on ICI-thyroiditis demonstrated severe destructive thyroiditis that was induced by anti-PD-1 antibody injections 2.5 months after Tg immunization. The administration of anti-PD-1 antibodies in that model resulted in an increase in the frequency of CD4+ T cells in the thyroid and cervical lymph nodes, but not CD8+ T cells. In another study irradiation recipient mice showed damage of the thyroid follicular architecture following adoptive transfer of CD4+ T cells from the cervical lymph nodes of mice with destructive thyroiditis [Iwama et al., 2022].

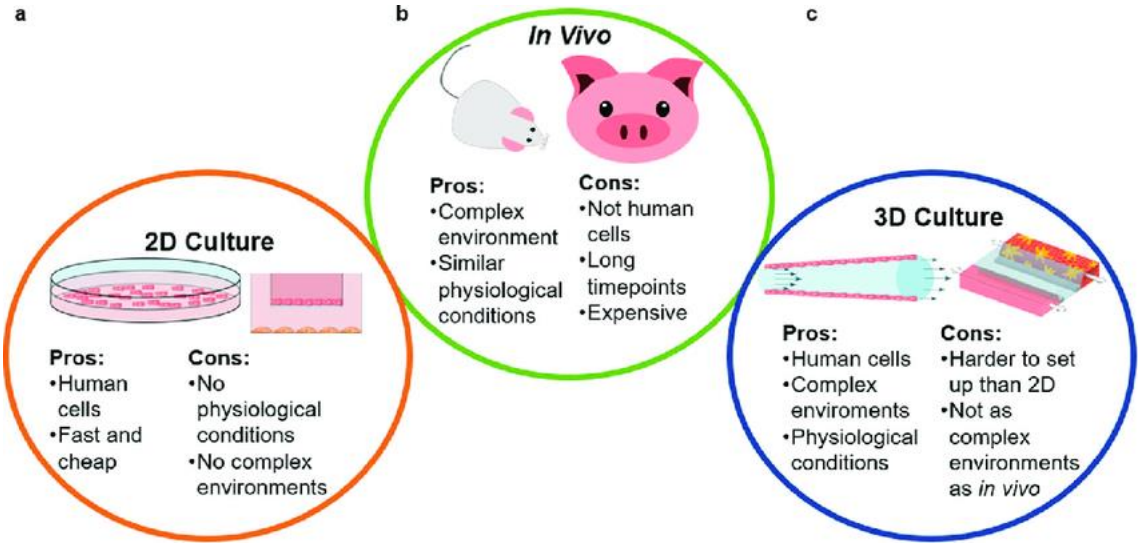

Figure 2.3: Advantages and disadvantages of in vitro models, such as 2D and 3D cultures, and in vivo. Extracted from [Andreeva et al., 2023].

However, it is important to acknowledge that the immune system components and responses of various species can lead to biased results that may not be truly applicable to human conditions. In vitro studies provide a controlled environment that facilitates the high-precision examination of cellular and molecular mechanisms. Common in vitro methods consist of 2D and 3D cultures. The 2D culture method entails the cultivation of cells in a monolayer, typically in a petri dish or well plate. This method is straightforward, cost-effective, and convenient for the observation and manipulation of cells. The absence of the complexity of the natural cellular environment may limit its applicability to in vivo conditions. 3D culture systems are gaining prominence as a more physiologically relevant models because of their capacity to more closely replicate the natural architecture and microenvironment of tissues. By employing these systems to simulate the interactions between cells and their extracellular matrix, a more realistic comprehension of cell behavior can be achieved [Pampaloni et al., 2007].

2.7.1 3D Co-culture System Employing Patients' Immune Cells

The implementation of advanced 3D culture models, such as thyroid spheroids, provides substantial benefits in the context of ICI-induced TD. The 3D spheroid culture system is designed to mimic the physiological method of cell culture. Next, it preserves structural integrity, which facilitates biomimicry. Third, there is a potential for

continuous communication with other cells, including immune cells. Co-cultures have consistently been a desirable experimental approach to more accurately represent the physiology [Keller et al., 2020]. The study that employed RAW264.7 cells (murine monocyte-macrophages line) and human PBMCs to investigate in vitro whether elevated iodine could cause macrophage polarization imbalance is one example of co-culture use in thyroid autoimmune studies [Cai et al., 2022].

The integration of patient-specific PBMCs into 3D thyroid spheroid cultures is a potent patient-specific approach. By employing a variety of techniques including and not limited to immunofluorescence, gene expression analysis, western blot, and flow cytometry, a comprehensive analysis of the co-cultures can be conducted to investigate the behavior of the immune cells of patients undergoing ICI therapy in the presence of the thyroid spheroids. Yet, it is critical to first optimize technical protocols using cell lines before completely transitioning to patient-specific models that utilize both patient thyroid cells for spheroid development and patient PBMCs which represents an autologous system. Unlike primary patient cells, which have a finite lifespan, cell lines exhibit stable properties over multiple passages, which allows for consistency and reproducibility. This stability suggests a consistent supply for long-term studies and mitigates variability, thereby improving the reliability of experimental results [Kaur and Dufour, 2012]. Furthermore, because fresh tissue samples or specialized conditions are not required, cell lines are less expensive, less sensitive to culture conditions, and easier to maintain. More ethical and personalized research approaches can be built upon the following techniques to better understand the pathophysiology of such conditions.

2.7.2 Nthy-Ori 3-1 Cell Line

The immortalized Nthy-ori 3-1 cell line is a human follicular epithelial cell line that is widely utilized in studies on autoimmune thyroid diseases, including HT.This cell line was generated by transfecting normal human thyroid cells with the large T antigen of the SV40 virus. This process enabled the cells to replicate indefinitely while preserving numerous typical thyroid cell characteristics. These cells express essential thyroid-specific markers and functions, including Tg, TPO, and the sodium/iodide symporter (NIS), which are essential for the synthesis and function of thyroid hormones. The SV40 large T antigen's integration enables continuous cell proliferation without the

limitations of senescence, rendering it a dependable and consistent model for long-term research [Fabien et al., 1994]. The Nthy-ori 3-1 cell line shows great potential as an in vitro model due to its distinct thyroid-specific traits and ease of manipulation. Thyroid follicular cells are the main cells affected in the destruction observed in ICI-induced TD, making this cell line particularly relevant for studying this condition.

2.8 Objectives

The primary objective of this research is to immunophenotype patients undergoing ICI therapy at two critical time points: immediately before therapy initiation and three weeks post-therapy, in light of the limited availability of immunophenotyping studies. In order to characterize immune cell populations, including T cells along with their subsets Th, CTLs, and Tregs, B cells, and NK cells, flow cytometry will be implemented. The TNF-α and IFN-γ expressions will be assessed to evaluate the inflammatory levels. Comparative analyses will be conducted to identify potential changes in the early phases of ICI-therapy in comparison to the control groups, which consist of healthy individuals and patients with Hashimoto's thyroiditis. This will help to identify the earliest patterns of immunological alteration that could potentially serve as predictive biomarkers for both clinical outcomes following the therapy and the development of irAEs, specifically ICI-induced TD.

The development and optimization of a novel 3D co-culture methodology are among the study's additional primary objectives. The Nthy-ori 3-1 cell line generated spheroids will be co-cultured with patient PBMCs, along with the corresponding control groups. This methodological study, which uses PBMCs from patients receiving ICI therapy as a case study, is justified by the scarcity of thorough co-culture procedures for this specific cell line and condition. The development of such model can also be adapted to investigate various thyroid diseases, including but not limited to ICI-induced TD. Flow cytometry will be employed in subsequent evaluations to examine the dynamics of potential cytotoxicity and immune cell infiltration within the co-cultures. Although the methodologies utilized in this investigation may not be applicable to clinical practice, their optimization and development have the potential to be adapted to autologous systems in the future.

Chapter 3:**METHODOLOGY**

3.1 Ethical Committee Approval

This study was conducted in accordance with the ethical guidelines outlined in the Declaration of Helsinki and gained approval from the Institutional Review Board (IRB) of Koç University (No. 2024.148.IRB2.070). Patients (n=9) who were subjected to ICI therapy, along with healthy control (n=6) and Hashimoto's thyroiditis (HT) control (n=3) groups, were recruited from Koç University Hospital between June 2024 and August 2024. All participants gave written informed consent prior to beginning the study. Complete information on the rights of potential participants, the objectives of the study, and the processes involved was provided. The inclusion criteria for the present study encompassed individuals aged 18 to 75, of either gender, who were required to receive ICI therapy, either as a standalone treatment or in conjunction with chemotherapy. Individuals having a history of autoimmune diseases and thyroid disorders were not included in this study. Healthy controls and patients with HT were selected based on age and gender matching criteria following the collection of patient samples. Both ICI-induced TD patients and HT control subjects were requested to provide blood samples as an integral part of their treatment regimen, thereby ensuring that this requirement did not cause any inconvenience.

3.2 Immunophenotyping of Patient and Control Samples

At the initiation of ICI therapy, peripheral blood samples were collected from patients and PBMCs were isolated. The technique was repeated three weeks later, which is the anticipated period for the development of ICI-induced TD [Karaviti, 2024]. At each time point, the hormone levels, including TSH, fT3, and fT4, were evaluated by biochemical analysis in the clinical laboratory of Koç University Hospital. Following the collection of patient samples, the blood collection and PBMC isolation technique was repeated on the control groups.

3.2.1 PBMC Isolation

In order to isolate PBMCs, a volume ranging from 3 to 15 mL of peripheral blood was collected from both patients and control subjects. The blood was drawn into tubes

containing K2-EDTA to avoid blood clotting. The whole blood was diluted with 1X PBS at room temperature in a 1:1 (v/v) ratio, ensuring complete mixing. The blood samples, which had been diluted, were gradually placed on top of Ficoll (Serumwerk Bernburg AG, 00223) at a ratio of 5 parts blood to 2 parts Ficoll, measured by volume. The mixture was then centrifuged at 2000 rpm for 20 minutes (acceleration 5, deceleration 1) at room temperature. The PBMCs, located at the interface between the plasma and the Ficoll layer, were carefully transferred to a new 15 mL Falcon tube using a Pasteur pipette (Figure 3.1). After adding 10 mL of RPMI-1640 (Capricorn, CP24-7051), the tube was centrifuged at 2000 rpm for 10 minutes (acceleration/deceleration max). The supernatant was discarded, and 10 mL of RPMI was added before another centrifugation with the same settings. The PBMCs were subsequently counted using a trypan blue-enhanced hemocytometer. A volume of 10 µL of the cell suspension dyed with trypan blue was transferred at the outer border of the hemocytometer. The cells were counted across all squares of the grid to derive an average count, and the concentration was determined using the following formula:

Cell concentration (cells/mL) = (Average cell count per square) × (Dilution factor) × (10^4).

The cells were frozen in 90% FBS with 10% DMSO at a concentration of approximately 3 × 10^6 cells/mL per cryovial and stored at -80°C until needed.

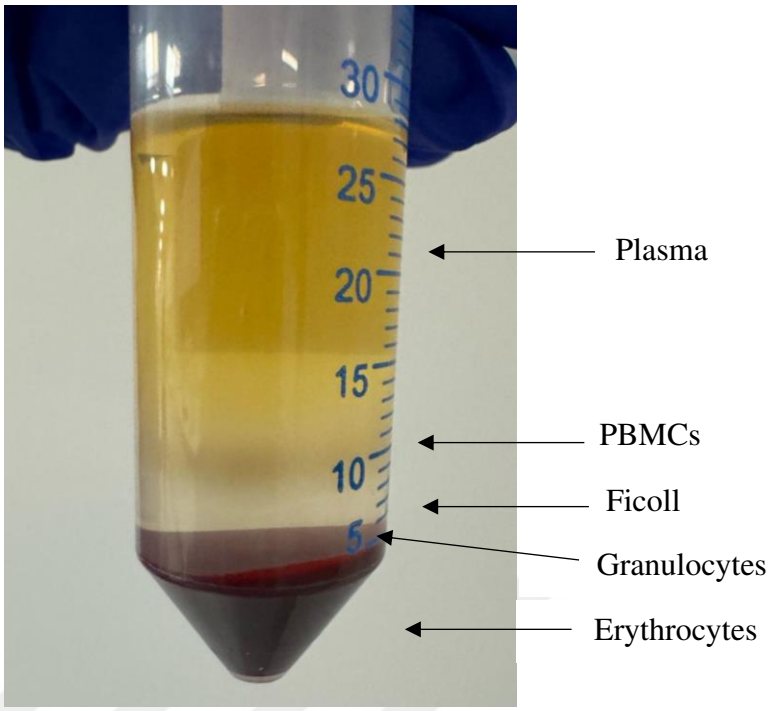

Figure 3.1: Density gradient based PBMCs isolation. The image displays the layers that result following centrifugation for 20 minutes at 2000rpm. The cloudy layer observed between the plasma and Ficoll consists of PBMCs.

Subsequently, the PBMCs were divided into two equal parts: one portion was used for immunophenotyping, while the other portion was frozen for additional investigations. Half of the PBMCs were stimulated for immunophenotyping with ionomycin, a calcium ionophore, and phorbol 12-myristate 13-acetate (PMA), an activator of protein kinase C. An inflammatory stimulus was employed to illustrate alterations in TNF-α as well as IFN-γ expression in both the patient and control samples, offering a comparative reference point for interpreting the response of each group.

3.2.2 PBMC Stimulation

PBMCs were thawed in a water bath and transferred into a 15 mL Falcon tubes containing 5 mL of complete medium, consisting of 90% RPMI-1640, 10% FBS, and 1% Penicillin/Streptomycin. The tubes were centrifuged at 500xg for 5 minutes at room temperature, after which the supernatant was discarded. The cell pellet was resuspended in 2 mL of 1X PBS and separated into two 12x75mm 5 mL FACS tubes

based on stimulated and unstimulated conditions. The cell concentrations for each tube were measured using an automatic cell counter. A total of 1-2 million PBMCs in each tube were centrifuged at 500xg for 5 minutes, and as much supernatant as possible was discarded. A 500X activation solution containing 40.5 μM PMA and 669.3 μM ionomycin was diluted to 1X with 100 μL of complete medium per well in order to activate the PBMCs. The activation solution was combined with 0.1 μL of Brefeldin A per 100 μL of media in order to trap TNF-α and IFN-γ inside the cells. Two 15 mL Falcon tubes were prepared, one with the media and activation solution combined, and the other with the media alone. The cells were then resuspended in 100 μL of the media including and excluding the activation solution for each tube of cells, and then placed into a 96-well round-bottom plate (Sarstedt, 1024321). After thorough mixing, the cells were incubated for 4 hours.

3.2.3 Flow Cytometry Analysis of Immune Subsets

Following the PBMC stimulation, the plate was centrifuged at 500xg for 5 minutes at room temperature before discarding the supernatant by rapidly inverting the plate in a single forceful motion. To stain non-viable cells, 100 μL of a solution containing 99 μL 1X PBS and 1μL Zombie NIR was added to each well, mixed thoroughly with a multichannel pipette, and incubated at room temperature in the dark for 10 minutes. The samples were centrifuged at 500xg for 5 minutes, with the supernatant being discarded. To achieve a final volume of 100 μl per sample, an antibody cocktail comprising 0.5 μL of each surface antibody (Table 3.1) in FACS buffer (0.5% BSA and 1X PBS) was prepared. The total volume of the antibody cocktail solution was determined by multiplying the volumes by the number of samples. After adding the antibody cocktail solution, the samples were allowed to incubate for 20 to 30 minutes at room temperature in the dark. The plate was centrifuged at 500xg for 5 minutes, then the supernatant was discarded. 200 μL of fixation buffer (4% w/v paraformaldehyde in 100 mL PBS) was added to the samples and incubated in the dark for 20 minutes. The samples were centrifuged using the same settings, and the supernatant was discarded. After adding 200 μL of permeabilization buffer (1X solution containing Triton X-100 and saponin), the supernatant was removed by another round of centrifugation. The cells were resuspended in 100 μL of permeabilization buffer with 1μl of TNF-α and IFN-γ *(Table*

3.1) added. Following a 20-minute dark incubation period, the solution allowed antibodies to bind to the intracellular targets. The plate was centrifuged with the same settings applied, and the supernatant was discarded. 500 µL of FACS buffer was introduced into 12x75mm 5 mL FACS tubes. Samples were resuspended in 100 µL FACS buffer and transferred to tubes for flow cytometry analysis by Cytoflex SRT Cell Sorter (Beckman Coulter, USA). Data analysis was performed using FlowJo FlowJo v.10.10.1 (BD Biosciences, USA).

Table 3.1: Antibodies used in the immunophenotyping by flow cytometry.

Target	Fluorophore	Clone	Brand/Catalog No
CD3	FITC	OKT3	BioLegend, 317306
CD4	PE-Dazzle 594	OKT4	BioLegend, 317448
CD8	Alexa Fluor 700	SK1	BioLegend, 344724
CD19	APC	HIB19	BioLegend, 302212
CD56	PE-Cy5	MEM-188	BioLegend, 304608
CD25	PE	BC96	BioLegend, 302640
CD127	Brilliant Violet 421	A019D5	BioLegend, 351328
IFN-γ	PE	B27	Biolegend/B271621
TNF-α	PE-Cy7	Mab11	Biolegend/B345903

3.3 Development of a Potential In-vitro 3D Co-culture Model with Nthy-Ori 3-1 Cells and PBMCs

The methodology for developing a prospective in-vitro model including 3D co-culture of thyroid cells (represented by the Nthy-Ori 3-1 cell line) and immune cells (particularly PBMCs) started with the initial culture of the cell line.

3.3.1 Nthy-Ori 3-1 Cell Culture

The cell line was kindly provided by Johannes Gutenberg University Mainz's molecular biology department. Nthy-Ori 3-1 cells were grown in a complete medium

containing 90% RPMI-1640 with L-glutamine (Capricorn, CP24-7051), 10% FBS, and 1% penicillin/streptomycin. First, Nthy-Ori 3-1 cells were thawed in a water bath at 37°C. Following this, the cell suspension was transferred to a 15 mL Falcon tube that contained 5 mL of pre-warmed complete medium. The tube was then centrifuged at 2000 rpm for 5 minutes at room temperature. Post-centrifugation, cells were seeded in a 25 cm^2 flask with 6 mL of complete media and kept at 37°C in a humidified 5% CO_2 atmosphere. Cell confluence determined the optimal ratio for cell passage, which was initially set at 1:3 for the first passage. Cell confluence was then monitored and changed, usually within 2 days for acceptable growth or 3–4 days if growth was insufficient. Upon attaining 80-90% confluence, the cells were prepared for 3D culture (Figure 3.2). After discarding the media, 1X PBS was used to rinse the cell monolayers. 1 mL of 0.25X Trypsin-EDTA (Multicell, 3255043224) was added, and the cells were left to incubate for 5 minutes at 37°C. The Trypsin-EDTA was neutralized by adding 5 mL of complete media after cell detachment was verified under a microscope. The contents of the flask were transferred to a 15 mL Falcon tube and centrifuged for 5 minutes at 2000 rpm. The cells were resuspended in 1 mL of complete medium after the supernatant was discarded. Using the Trypan Blue exclusion method, cells were counted, and the concentration needed for generating spheroids was determined.

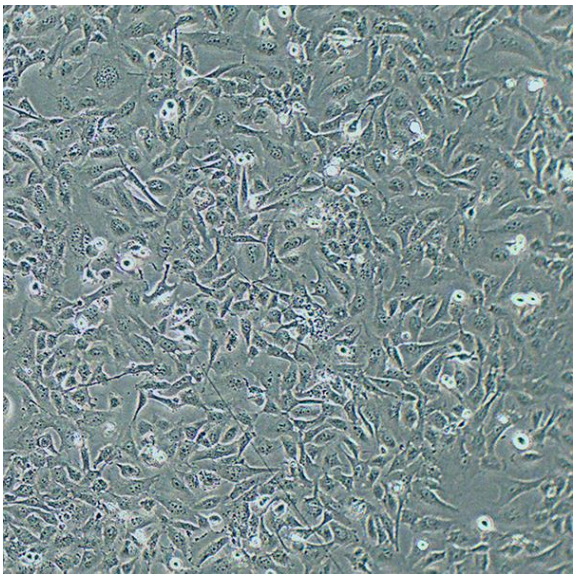

Figure 3.2: An image depicting a confluence of Nthy-Ori 3-1 cells above 90%.

3.3.2 Nthy-Ori 3-1 Spheroids Generation Using Agarose Coating Method

Various concentrations of Nthy-Ori 3-1 cells, specifically 1000, 2500, and 5000 cells, were transferred onto a 96-well round-bottom plate (Sarstedt, 1024321) using the agarose coating technique. Initially, 50 µL of agarose was applied to each well, and half of the volume was removed to generate a thinner coating, enhancing visualization. For half an hour, the agarose was left to cool and solidify. Next, Nthy-Ori 3-1 cells suspended in 150 µL of complete medium were added to each well, and the plate was incubated at 37°C in a humidified atmosphere with 5% CO2. On the third day, 100 µL of medium from each well was withdrawn and replaced with a fresh complete medium. Spheroids were completely assembled on day 4, which allowed for the subsequent assembly of a 3D co-culture system. Images were taken every other day, starting from day 1 of spheroid formation, using the Leica DMi3 microscope to examine the diameter and shape of the spheroids. ImageJ, an open-source image analysis software, was employed to determine the diameters of the spheroids. Measurements were obtained from 5 spheroids under each condition (1000, 2500, and 5000 cells), and the mean diameter was computed.

3.3.3 Viability Assessment

A viability assessment was performed using a 3-(4,5-dimethylthiazol-2-yl)-2,5-diphenyltetrazolium bromide (MTT) (Invitrogen, 250193) assay on days 4, 7, 10, 14, and 21, following the methodology described in the study by [Brochado, 2023]. Spheroids were transferred in triplicate to a flat-bottom 96-well plate (Sarstedt, 1024321), suspended in 100 µL of complete medium, assuring no disturbance of the spheroid structure by microscope examination, with previously specified conditions: 1000, 2500, and 5000 cells. Throughout each step, precautions were taken to protect the samples from exposure to light in order to prevent the MTT reagent from photodegrading. To eliminate any bias in the absorbance data, it was critical to prevent the formation of bubbles and verify that the media volume in each well was equal. After adding 100 µL of media containing the spheroid to each well, a 50 µL aliquot of 5 mg MTT powder per 1 mL of sterile 1X PBS solution was added. The plate was then incubated for 3 hours. In order to prevent aspirating the spheroid structure, the MTT solution was disposed of with caution. 100 µL of DMSO was introduced to each well

containing spheroids in order to dissolve the formazan crystals (Figure 3.3). With absorbance set to 570 nm, the plate was then read using Synergy H1 microplate reader.

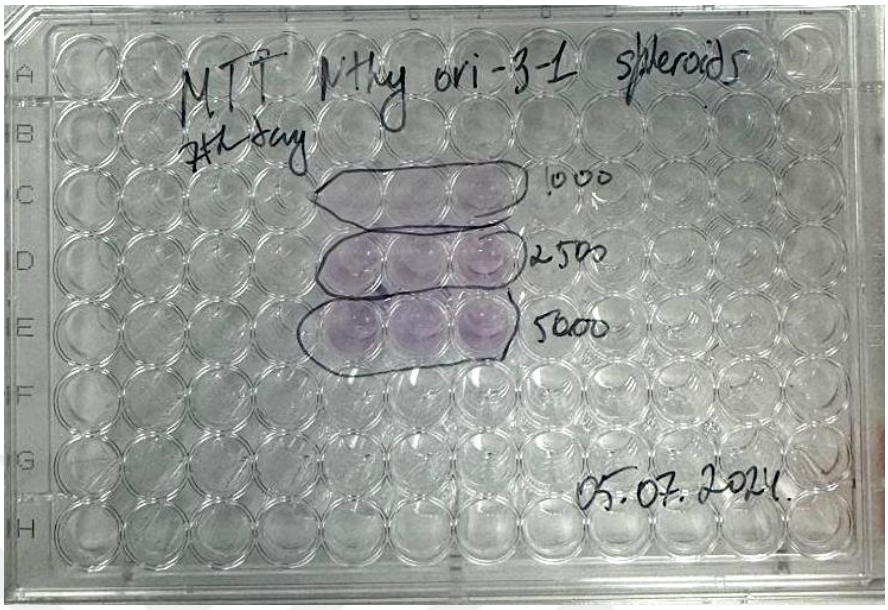

Figure 3.3: A 96-well plate containing spheroids composed of 1000, 2500, and 5000 cells, with the purple color corresponding to the dissolving Formazan crystals after adding DMSO.

3.3.4 Immunofluorescent Staining

Immunofluorescence was conducted on days 4, 14, and 21. 5 to 10 spheroids were collected in 1.5 mL Eppendorf tubes and subjected to a quick centrifugation (30 seconds at 700xg, 4°C) to settle the spheroids at the bottom. After removing as much media as possible without aspirating or disrupting the spheroid structure, as confirmed by microscopy, 1 mL of 1X PBS was added. Then, the tubes were subjected to centrifugation for a duration of 10 minutes at 700xg, 4°C. After discarding the supernatant, the cells were fixed with 500 µL of 4% PFA for 30 minutes at 4°C. The tubes were then centrifuged under the same settings, and the supernatant was discarded. The antibody solution was made by combining 60 µL of 1X PBS with 10 µL of DAPI mounting solution (Abcam, 1041148-3) and 1.5 µL of Phalloidin (Cayman, 06763592) per sample. The solution was introduced into the Eppendorf tubes and subjected to a 1-hour incubation at room temperature under light-restricted conditions. After incubation, 1 mL of 1X PBS was added, and the samples were centrifuged under the same conditions. The spheroids were then resuspended in 50 µL of 1X PBS. 10 µL of 1X PBS

containing spheroids were placed on a Nunc Glass Base Dish (Thermo Scientific, 150680) with circles drawn with PapPen to form a hydrophobic barrier and prevent the leakage of the spheroids (Figure 3.4).

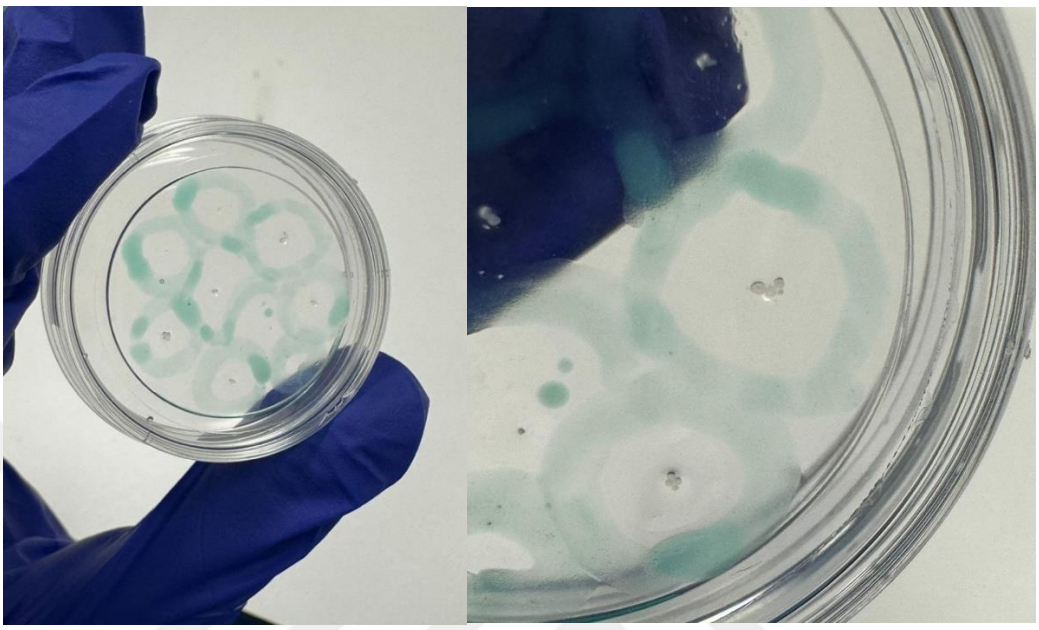

Figure 3.4: The glass dish with spheroids inside the hydrophobic circles.

3.3.5 Confocal Microscopy Imaging and Cell Counting

The stainings were visualized using a Leica DMI8-SP8 Confocal Microscope equipped with an HC PL FLUOTAR 10x/0.30 DRY objective and Leica Application Suite (LASX) software. PMT1 and PMT2 detectors as well as solid lasers 405 and 552 were used. The images were captured using a 10X magnification, 2048x2048 format, and Frame Accumulation 2 settings. Z-stack videos were captured in 20 steps, and for additional picture analysis, the maximum projection images with the least amount of background noise were utilized. Using Fiji software, images with DAPI-stained nuclei were examined in order to count the number of cells. Firstly, the images were imported into Fiji and then transformed into grayscale 8-Bit format. The 3D Gaussian Blur filter was applied to reduce the background noise, and subsequently, the nuclei were automatically counted by employing the "3D objects counter" setting.

3.3.6 CFSE Labelling of PBMCs for Visualization and 3D Co-culture

Using a Leica DMi8 microscope, the rate of PBMCs infiltration was observed before co-culturing with patient samples to provide a clear picture of the potential

infiltration patterns. In order to accomplish this, PBMCs from the control sample were labeled using the fluorescent dye CFSE (Carboxyfluorescein Diacetate Succinimidyl Ester). The PBMCs were first thawed and then transferred to a 15 mL Falcon tube with 5 mL of complete medium. After centrifuging the tube for 5 minutes at 500xg, the supernatant was discarded. The cell pellet was resuspended in 1 mL of 1X PBS containing 1 µL of CFSE dye followed by a 15-minute incubation at 4°C on the shaker. The tube was then filled with 4 mL of media, which was then centrifuged at 2000 rpm for 10 minutes at room temperature. The supernatant was discarded, and the cells were resuspended in 1 mL of complete medium and counted with Trypan blue. Co-culture with PBMCs began on the fourth day, when the spheroids had fully formed. For each well containing spheroids, 150 µL of PBMCs suspension in complete medium was gradually added after the initial medium was removed. Based on the assumption that 2500 cells are the optimum amount for Nthy-Ori 3-1 spheroids seeding, co-culture with PBMCs was performed at ratios of 1:0.5, 1:1, 1:2, and 1:5. After a 48-hour incubation period, the co-cultures were visualized.

After determining the optimal co-culture rate of 1:2, 3D co-culture was carried out with PBMCs of ICI-induced TD patients, patients without TD, and control groups. Following 48 hours of incubation, the co-cultures were ready for flow cytometry analysis.

3.3.7 Flow Cytometry of 2D and 3D Co-cultures

In each well of a 24-well plate, 500,000 Nthy-Ori 3-1 cells were seeded in 1 mL of complete medium for the 2D co-culture experiment. The cells were allowed to attach for 2 days during incubation before being co-cultured at a 1:1 ratio with patient and control PBMCs. Incubation of co-cultures continued for an additional 2 days. Following the incubation period, the media containing the cells was gathered into 15 mL Falcon tubes. Subsequently, the wells were filled with 500 µL of Trypsin-EDTA for 3 minutes to detach Nthy-Ori 3-1 cells. Once 4 mL of complete media had been added to the Trypsin, the detached cells were transferred to the corresponding Falcon tubes. These tubes were centrifuged at room temperature for 5 minutes at 2000 rpm. After discarding the supernatant, 1 mL of 1X PBS was added, and the mixture was then put into

12x75mm, 5 mL FACS tubes. A 5-minute centrifugation at 500xg was performed on these tubes. The supernatant was discarded and 100 µL of remained solution was mixed with 1 µL of Zombie NIR. The tubes were left in the dark for a period of 10 minutes. The cells were then washed with 1 mL of FACS buffer, and the surface staining was carried out with 0.5 µL of each antibody in 100 µL of FACS buffer. Prior to the final wash, the tubes were incubated in the dark for 20 minutes. After adding 500 µL of FACS buffer to a cell pellet, the tubes were ready for flow cytometry analysis using the Cytoflex SRT Cell Sorter (Beckman Coulter, USA) and FlowJo v.10.10.1 (BD Biosciences, USA) for data analysis.

For the spheroid co-cultures, each 2500 cell spheroid was co-cultured with 5000 PBMCs (at a 1:2 ratio) for 48 hours. Next, a P1000 pipette was used to transfer the co-cultures (16 per sample) to 1.5 mL Eppendorf tubes. After allowing the spheroids to settle at bottom of the tubes for 5 minutes, the whole medium was carefully taken out, leaving only the spheroids that had PBMCs infiltrated. The spheroids were then disrupted with 500 µL of Trypsin-EDTA and gentle pipetting before incubation for 5 minutes. The procedure was repeated for 5 more minutes if, as determined by microscopy, a single cell suspension could not be obtained. The single cell suspension was confirmed using microscopy after the cell suspension was passed through a 45 µm cell strainer. For a period of 5 minutes, the tubes were centrifuged at 500xg. After discarding the supernatant, the cells were resuspended in 1 mL of 1X PBS and then put into 12x75mm, 5 mL FACS tubes. Then, the tubes went through a 5-minute centrifugation run at 500xg. Following the removal of the supernatant, 1 µL of Zombie NIR was added to 100 µL of remained 1X PBS. The tubes were then left to incubate for 10 minutes in the dark. The surface staining was conducted using the same methodology as for the 2D co-cultures, after the cells were washed with 1 mL of FACS buffer.

Table 3.2: Antibodies used in immunophenotyping of 2D and 3D co-cultures.

Target	Fluorophore	Clone	Brand/Catalog No
CD45	PE-Cy7	2D1	BioLegend, 368532
CD3	FITC	OKT3	BioLegend, 317306
CD4	PE-Dazzle 594	OKT4	BioLegend, 317448
CD8	Alexa Fluor 700	SK1	BioLegend, 344724
CD19	APC	HIB19	BioLegend, 302212
CD56	PE-Cy5	MEM-188	BioLegend, 304608

Chapter 4:**RESULTS**

4.1 Patient Characteristics

This study comprised 9 (n=9) patients who were about to start ICI therapy either alone or in combination with chemotherapy (Table 4.1b). The patients' blood was obtained for immunophenotyping at two significant time points: immediately before treatment and three weeks later. In addition, thyroid hormone levels, specifically TSH, fT3, and fT4, were assessed to elucidate potential TD development (Table 4.1a).

Table 4.1: (a) Patients' thyroid hormone levels and potential TD development. In the clinical laboratory where the measurements were performed, the following adult reference ranges were used: TSH: 0.40-5.10 uIU/mL, fT4: 0.93-1.7 ng/dL, fT3: 2.04-4.4 pg/dL.

Patient №	Thyroid hormone before therapy			Thyroid hormones after three weeks of therapy			Potential TD following ICI therapy
	TSH(uIU/mL)	fT3 (pg/mL)	fT4 (ng/dL)	TSH (uIU/mL)	fT3 (pg/mL)	fT4 (ng/dL)	
1	1.33	2.05	1.21	2.26	2.28	1.3	No
2	2.98	3.59	1.14	1.48	2.42	1.29	No
3	2.53	2.61	1.30	0.81	3.32	1.65	Thyrotoxicosis
4	0.47	2.94	1.89	0.91	2.11	1.61	No
5	2.98	2.79	1.16	2.02	2.83	1.40	No
6	1.29	3.47	1.24	1.79	3.41	1.16	No
7	1.8	1.93	1.32	1.62	2.59	1.31	No
8	2.22	2.71	1.03	2.15	1.11	3.08	Hormonal dysregulation
9	0.42	3.79	18.10	0.29	4.14	16.90	No

(b) Patients' clinical data.

Patient №	Gender	Age	Therapy	ICI Type	Cancer Type	Stage	Metastases	Family history of cancer	Comorbidities	BMI
1	Male	62	Keytruda + chemotherapy	PD-1	Lung cancer (Adenocarcinoma)	IV	Yes	Adenocarcinoma (mother's side)	Chronic pancreatitis Cataract surgery	23.59
2	Female	35	Keytruda	PD-1	Triple negative breast cancer	I	No	Breast cancer (relatives)	Not identified	20.31
3	Male	60	Keytruda + chemotherapy	PD-1	Lung cancer (Squamous cell carcinoma)	IV	Yes	Lung cancer (mother's side)	Hodgkin lymphoma (2000) Tongue SCC(2022) Splenectomy(2020)	35.03
4	Female	72	Atezo	PD-L1	Lung cancer (Small cell adenocarcinoma)	I	No	Not identified	Hypertension Hyperlipidemia Diabetes Mellitus Coronary artery disease	30.02
5	Male	41	Keytruda	PD-1	Renal cell carcinoma	Not identified	No	Not identified	VP shunt in the brain (2007) Aquaductus cerebri occlusion Pilonidal sinus operation (2005)	29.07

6	Male	33	Keytruda	PD-1	Malignant Melanoma	IIIC	No	Not identified	Not identified	36.00
7	Male	68	Keytruda	PD-1	Lung cancer (Adenocarcinoma)	IV	Yes	Colon cancer (mother's side)	Diabetes Mellitus Coronary artery disease	28.73
8	Male	44	Keytruda	PD-1	Recurrent malignant melanoma	IIIC	Not assessed	Endometrium cancer Breast cancer (relatives)	Hypertension	33.43
9	Male	71	Opdivo + chemotherapy	PD-1	Lung cancer (Squamous cell carcinoma)	III	Not assessed	Lung cancer (relatives)	Hypertension Benign prostate hyperplasia	18.56

All of the patients received different types of ICI drugs for the treatment of various types of tumors, with anti-PD-1 therapy (Keytruda) and lung carcinoma being particularly prevalent. Based on the clinical data, patient №9 was found to have hyperthyroidism due to the initially elevated fT3 and fT4 levels and the suppressed TSH levels. This patient was excluded from the statistical analysis because of the disagreement with established exclusion criteria which implies not having thyroid disorders before therapy. ICI-induced TD was suspected for patients №3 and №8. Keytruda, an anti-PD1 therapy, was administered to both patients, while patient №3 received it in combination with chemotherapy.

A 44-year-old male (Patient №8) with recurrent malignant melanoma, classified as Stage IIIC, and a 60-year-old male (Patient №3) with Stage IV lung cancer, specifically squamous cell carcinoma with verified metastases, are both presenting complex oncological profiles. The medical history of patient №3 is particularly complex due to the history of Hodgkin lymphoma in 2000, squamous cell carcinoma of the tongue in 2022, and a splenectomy conducted in 2020. Patient №8 has been challenged with hypertension. The BMI of both of these patients is over 30, which is classified as obese.

A typical picture of subclinical thyrotoxicosis following ICI therapy is displayed by Patient №3, whose TSH levels of 0.81 uIU/mL (0.40-5.10 uIU/mL) were suppressed on the third week after therapy initiation with an initial uIU/mL of 2.53. In patient №8, the hormonal status is clearly dysregulated, as fT3 levels 1.11 pg/dL (2.04-4.4 pg/dL) were dropped and fT4 levels 3.08 pg/dL (0.93-1.7 ng/dL) were elevated.

After collecting the blood samples from the patients, age and gender matched healthy controls (n=6) were selected. HT controls (n=3), in turn, functioned as autoimmune positive controls (Table 4.2).

Figure 4.2: Control subjects' characteristics.

Healthy controls		**Hashimoto's Thyroiditis controls**	
Gender	**Age**	**Gender**	**Age**
Female	45	Female	54
Male	62	Female	57
Female	64	Female	69
Male	60		
Male	69		
Male	72		

4.2 Immunophenotyping of Peripheral Blood of Patient and Control Samples

Flow cytometry was performed on both patient and control samples to evaluate any potential variations in immune cell populations before and three weeks after ICI therapy, as well as corresponding control groups consisting of healthy individuals and HT controls. An appropriate gating strategy was used to identify B cells, NK cells, T cells, including their subtypes CTLs and Helper T cells (or THLs), and Tregs (Figure 4.1a). IFN-γ and TNF-α levels as well as their expression intensities were analyzed in B cell, CTL, THL, NK, and NKT-like cell populations (Figure 4.1b). The following gating strategy was applied to all of the samples.

(a)

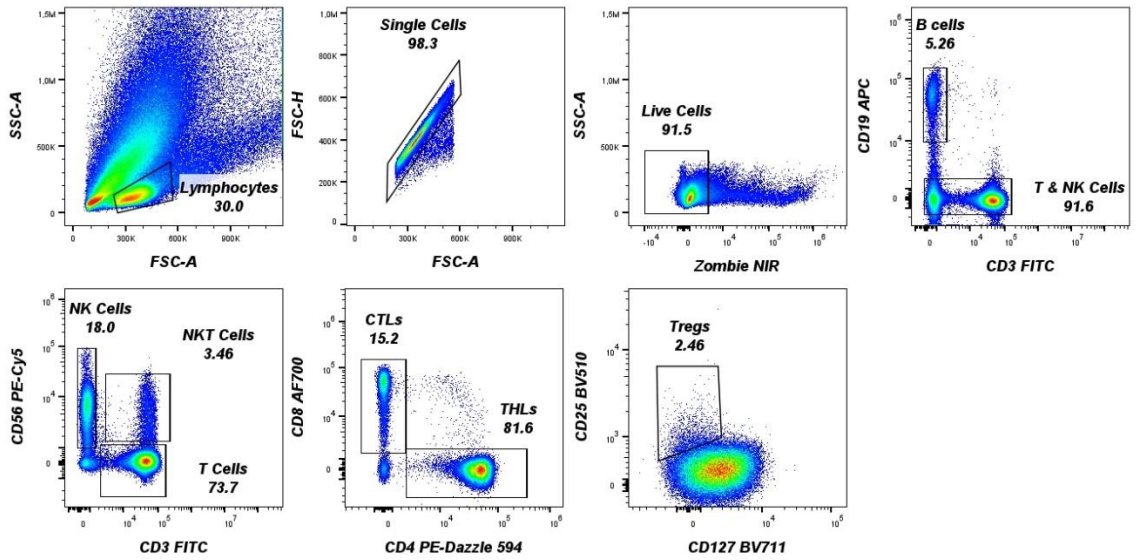

(b)

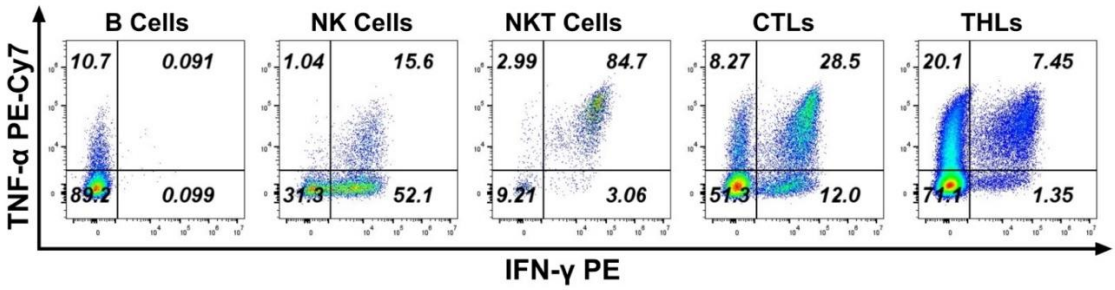

Figure 4.1: Flow cytometry gating strategy:

(a) The lymphocytes were gated based on the size and granularity (FCS-A versus SSC-A). Doublets were excluded and live cells (Zombie NIR-) were gated by plotting the viability dye (Zombie NIR) against SSC-A. Within the lymphocyte population, B cells (CD19+ and CD3-) as well as T cells and NK cells were identified (CD3+). Within T and NK cell populations, by plotting CD3 versus CD56: NK cells (CD56+ CD3-), NKT-like cells (CD3+ CD56+) and T cells (CD3+CD56-) were distinguished. CTLs (CD8+ T cells) and THLs (CD4+ T cells) were further gated within T cell population. Tregs, in turn, were distinguished by CD25+ and CD127- gating. (b) IFN-γ and TNF-α produced by CTLs, THLs, NK cells, NKT-like cells, and B cells were gated within corresponding immune cell populations (IFN-γ versus TNF-α).

4.2.1 Statistical Analysis

Following flow cytometry, FlowJo analysis was used to generate the appropriate calculations for each immune cell group in each sample for statistical analysis with GraphPad Prism 10.2.3. The data analysis initially focused on patients with ICI-induced TD, specifically №3 and №8, to look for variations in immune cell makeup, IFN-γ and TNF-α levels, and expression intensities before therapy and three weeks after, when the TD developed. There were no statistically significant differences ($p \geq 0.05$) in any of these variables (Figure 4.2).

(a)

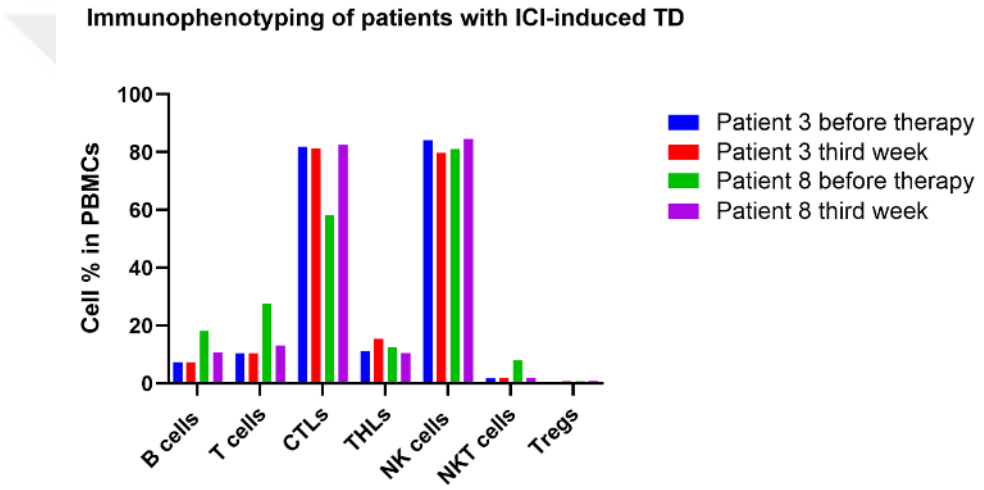

(b)

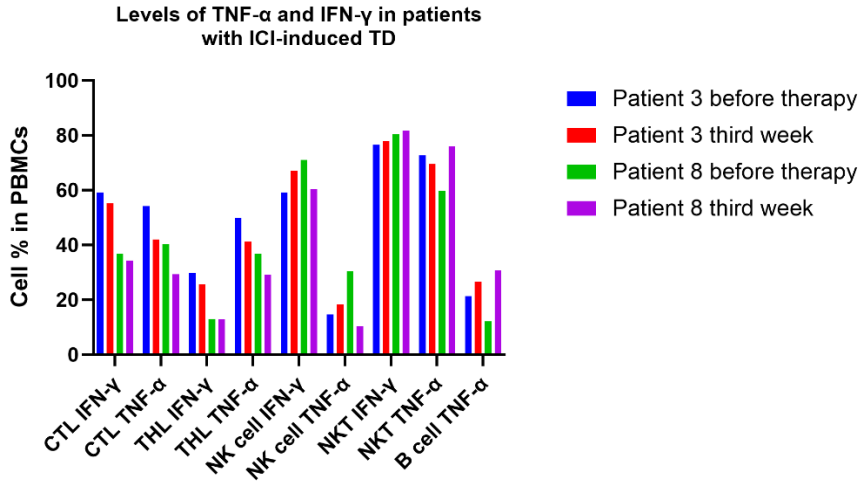

(c)

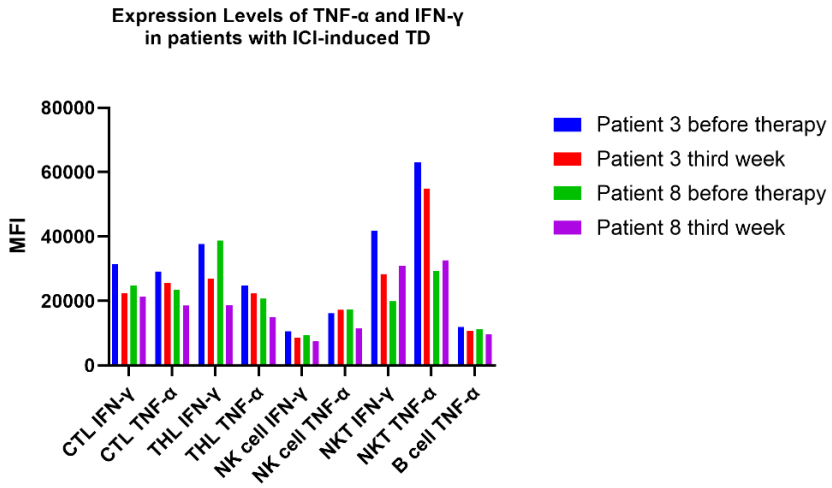

Figure 4.2: Graphs generated as a result of statistical analysis of data from patients №3 and №8 prior to and three weeks following therapy:

(a) The percentage of immune cells in PBMCs, including B cells, T cells, CTLs, THLs, NK cells, NKT-like cells, and Tregs, did not show any statistically significant differences ($p \geq 0.05$).

(b) and (c) The levels (%) and expression intensity (MFI) of IFN-γ and TNF-α did not show any statistically significant differences ($p \geq 0.05$).

Graphs were created with GraphPad Prism 10.2.3, and 2-way ANOVA with post-hoc Tukey's test was utilized for statistical analysis.

Following the analysis of ICI-induced TD patients, the investigation focused on potential differences within all patient samples (n=8) before and three weeks after receiving the treatment (Figure 4.3). The analysis revealed no significant differences ($p \geq 0.05$) in immune cell composition, however, IFN-γ and TNF-α levels and expression intensities differed. After three weeks of ICI therapy, IFN-γ levels produced by CTLs and NK cells were significantly increased ($p \leq 0.05$), while TNF-α levels were significantly increased ($p \leq 0.05$) by B cells, suggesting an increase in inflammation levels in patients.

(a)

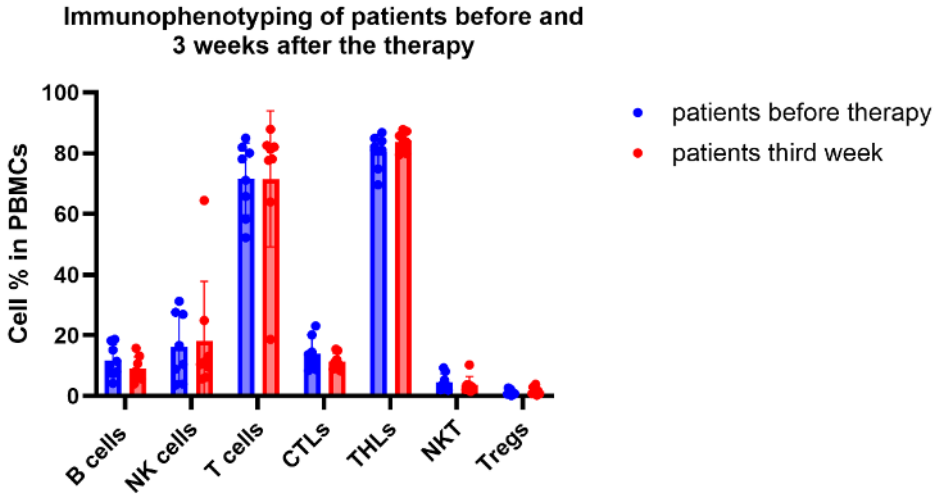
Immunophenotyping of patients before and 3 weeks after the therapy
Cell % in PBMCs
100
80
60
40
20
0
B cells
NK cells
T cells
CTLs
THLs
NKT
Tregs
patients before therapy
patients third week

(b)

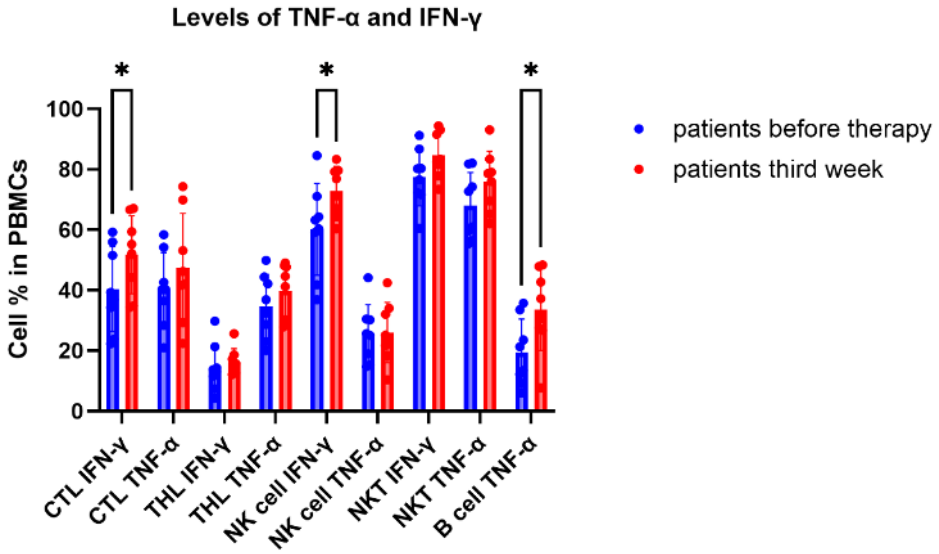
Levels of TNF-α and IFN-γ
Cell % in PBMCs
*
*
*
100
80
60
40
20
0
CTL IFN-γ
CTL TNF-α
THL IFN-γ
THL TNF-α
NK cell IFN-γ
NK cell TNF-α
NKT IFN-γ
NKT TNF-α
B cell TNF-α
patients before therapy
patients third week

(c)

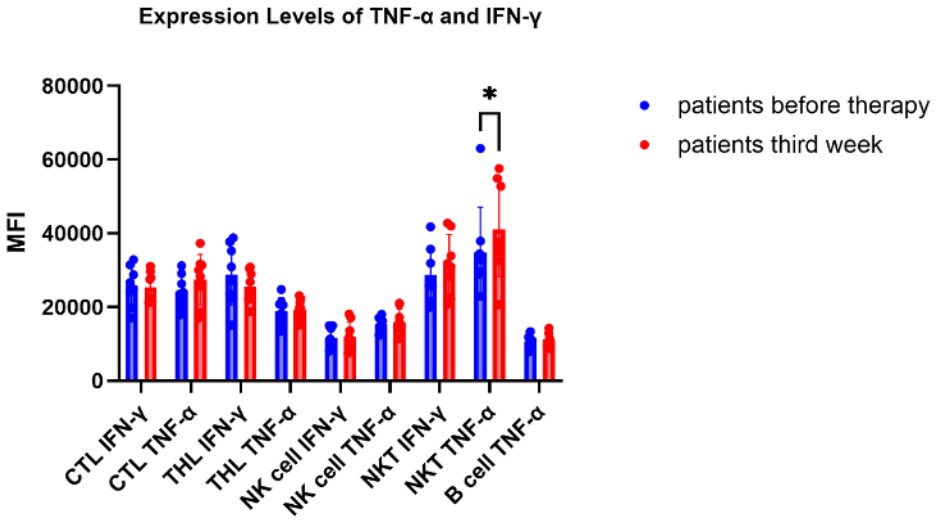

Figure 4.3**:** Immunophenotyping and IFN-γ and TNF-α levels in patients before and after three weeks of therapy:

(a) No significant variations ($p \geq 0.05$) in the percentages of immune cell subsets (CD4, CD8, CD19, NK, NKT-like cells, and Treg cells) between time periods.

(b) After three weeks of therapy, IFN-γ levels are significantly increased ($p \leq 0.05$) in CTL and NK cell populations; TNF-α levels are significantly higher ($p \leq 0.05$) in B cells.

(c) A significant increase ($p \leq 0.05$) in TNF-α expression in NKT-like cells, as evidenced by an apparent rise in MFI. Statistically significant results are marked by asterisks (*). Graphs were created with GraphPad Prism 10.2.3, and 2-way ANOVA (repeated measures) with post-hoc Tukey's test with was utilized for statistical analysis.

Finally, statistical analysis was conducted on all research groups, which included patient samples (n=8), healthy (n=6), and HT (n=3) control samples (Figure 4.4). The analysis found no significant difference in immune cell composition across all sample groups ($p \geq 0.05$, Figure 4.4a). HT controls had significantly greater IFN-γ and TNF-α levels and expression intensities ($p \leq 0.05$) than other groups. This is a predicted trend, given that HT controls have established immunological dysregulation defined by the presence of autoimmune condition.

After three weeks of therapy, there were significantly higher levels ($p \leq 0.05$) of TNF-α produced by patients' B cells (Figure 4.4 b and c).

(a)

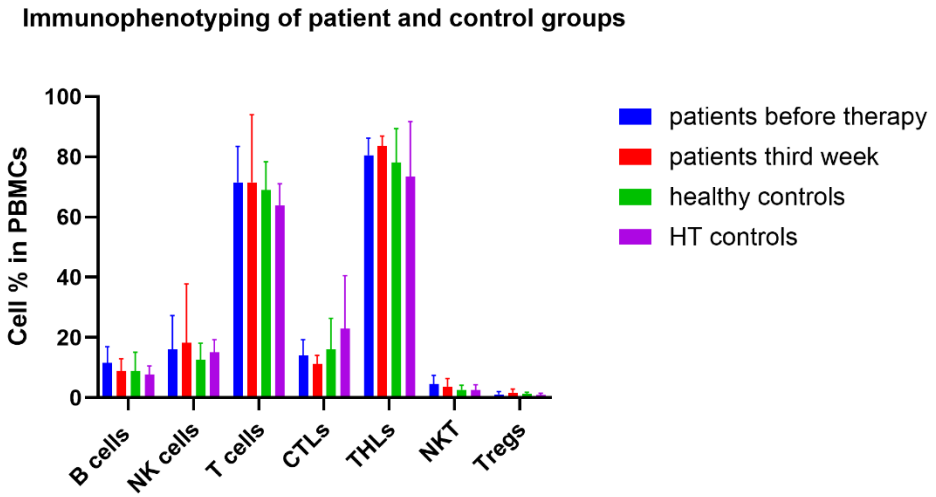

(b)

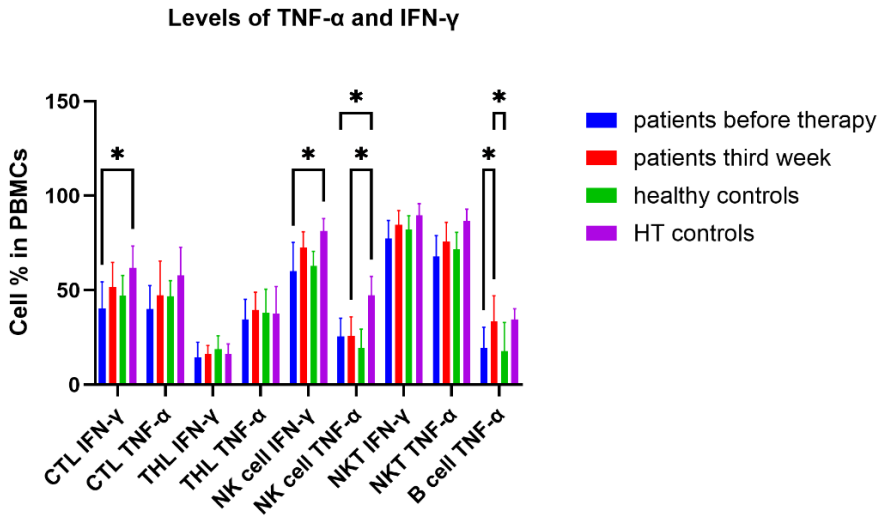

(c)

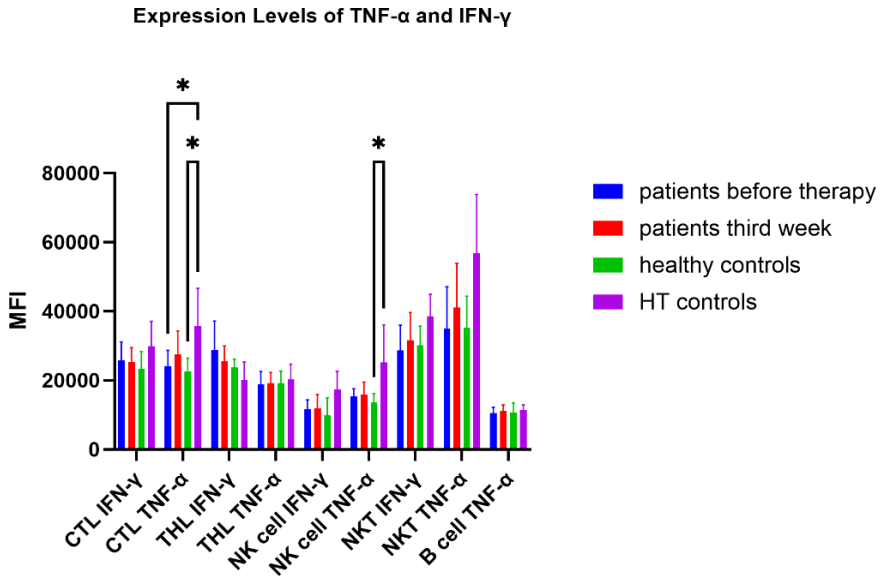

Figure 4.4: Immunophenotyping and IFN-γ and TNF-α levels in patient as well as control groups:

(a) There are no statistically significant variations ($p \geq 0.05$) in immune cell composition between the groups.

(b) IFN-γ levels produced by CTLs and NK cells of HT controls are significantly higher ($p \leq 0.05$) than in patients prior to therapy. TNF-α levels produced by NK cells of HT controls are significantly higher ($p \leq 0.05$) than those in healthy individuals and patients prior to therapy. In addition, there is a statistically significant increase ($p \leq 0.05$) in TNF-α of patients' B cells after three weeks of therapy compared to healthy controls and before therapy.

(c) TNF-α expression in CTLs is statistically higher ($p \leq 0.05$) in HT controls than in patients before therapy or in healthy individuals. TNF-α expression in NK cells is significantly higher ($p \leq 0.05$) in HT controls than healthy controls. Statistically significant results are marked by asterisks (*). Graphs were created with GraphPad Prism 10.2.3, and 2-way ANOVA (repeated measures) with post-hoc Tukey's test was utilized for statistical analysis.

Overall, significant changes were found in the levels and expression intensities of IFN-γ and TNF-α in patients before and after therapy, as well as when compared to the

control groups (TNF-α produced by B cells). However, these tendencies were not detected when comparing two patients who had TD, due to the limited sample size.

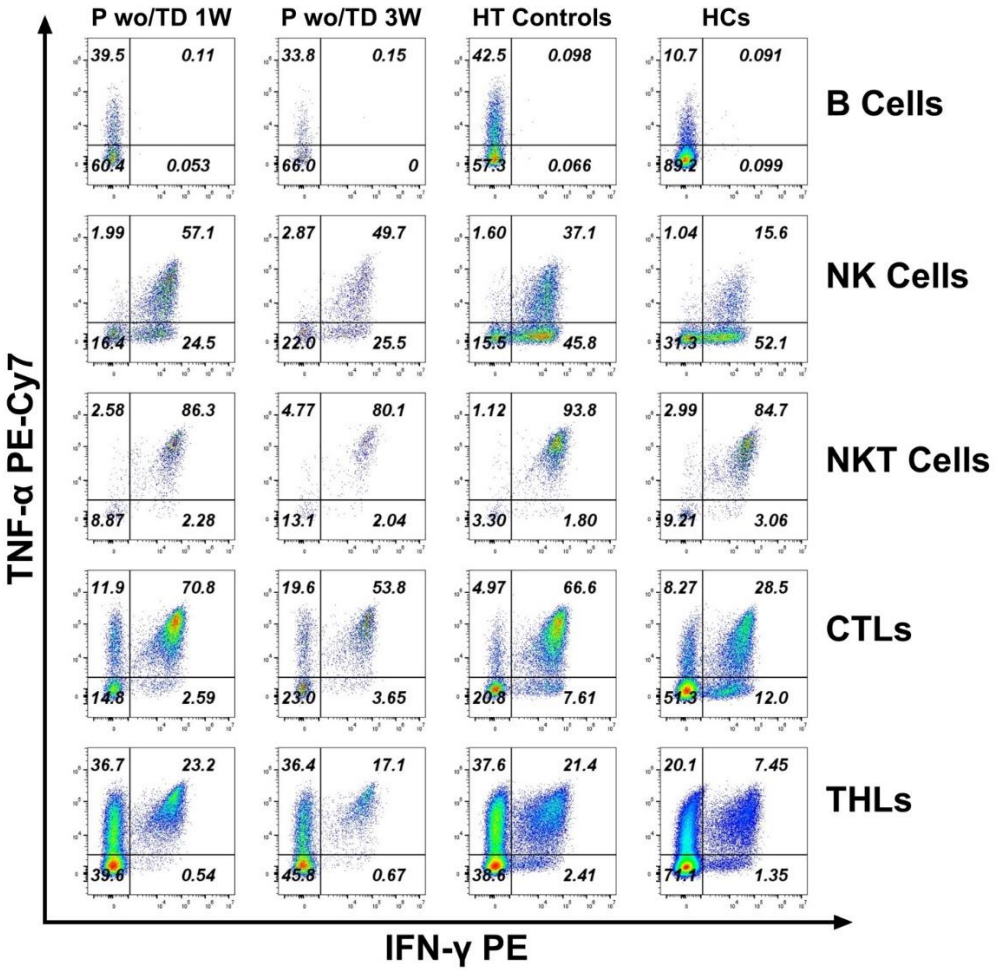

Figure 4.5: Flow charts for visual comparisons of IFN-γ and TNF-α levels.

In this graphical representation, the flow charts of patients without TD before and 3 weeks after therapy (P wo/TD), as well as healthy controls (HC) and Hashimoto's thyroiditis controls (HT), were chosen at random to enhance visual comparability.

4.2.2 3D Co-culture Model Development

The 3D co-culture model was created to investigate ICI-induced TD by culturing Nthy-Ori 3-1 spheroids using an agarose coating method and co-culturing with PBMCs from patient and control samples. The objective was to determine the potential for immune cell infiltration into the spheroid structures and the impact of PBMCs on the viability of spheroids, which may represent the cytotoxicity levels within co-cultures.

The initial phase of model development involved the optimization of all technical protocols.

4.2.3 Nthy-Ori 3-1 Spheroids' Characteristics

The Nthy-Ori 3-1 spheroids were cultivated at an initial cell count of 1000, 2500, and 5000 cells per well. The complete formation of spheroids occurred on the fourth day post-seeding. Subsequently, the diameter of the spheroids was measured on days 4, 7, 10, 14, and 21 using ImageJ to produce a growth kinetics graph (Figure 4.5a). Further, morphological alterations were documented throughout the 21-day incubation period (Figure 4.5b).

(a)

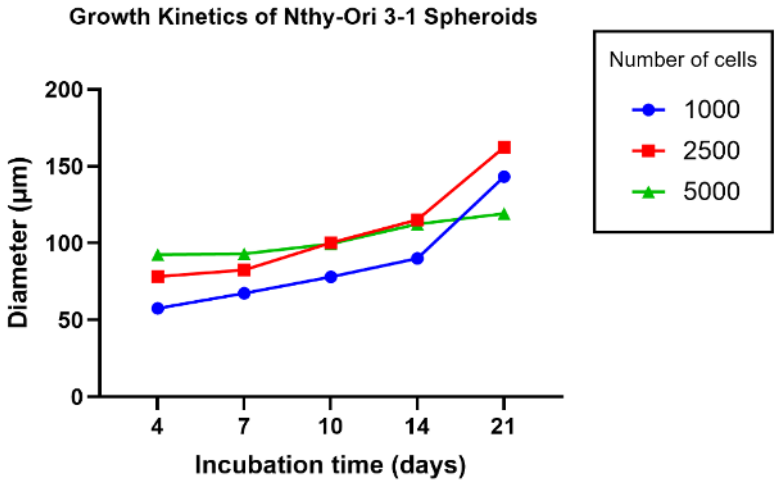

(b)

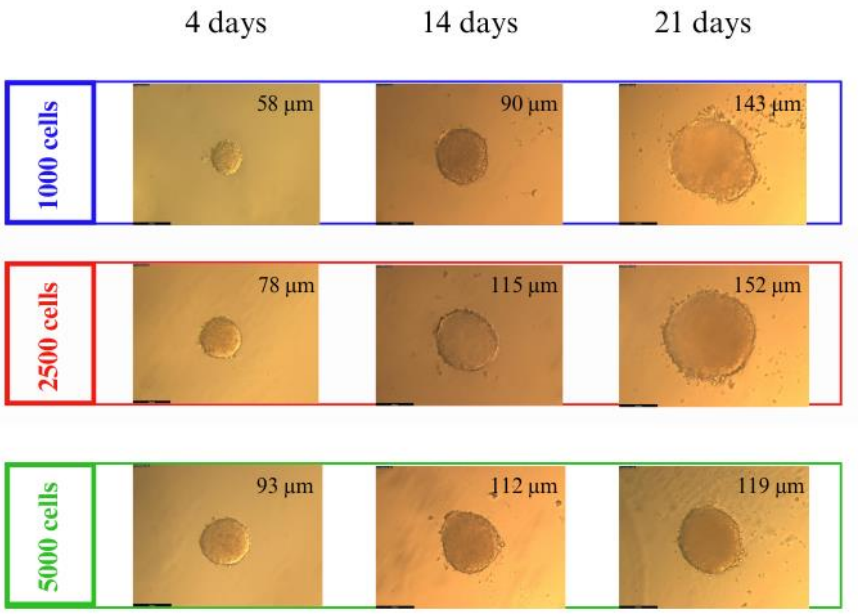

Figure 4.6: Spheroids' characteristics:

(a) The growth kinetics of Nthy-Ori 3-1 spheroids are presented by plotting the incubation time (days) against the spheroid diameter (µm) for initial cell counts of 1000, 2500, and 5000 cells. The graph was created using GraphPad Prism 10.2.3.

(b) Morphological changes that correspond to these cell numbers over three time intervals, namely 4, 14, and 21 days.

ImageJ software was employed to analyze 5 spheroids per condition in order to determine the mean spheroid diameters. The mean diameters of the spheroids on day 4 were directly proportional to the number of cells seeded, with the greatest diameter achieving 93 µm at 5000 cells. Across all cell densities, spheroids were properly shaped and small in size. Spheroids continued to grow, with a modest increase in diameter, on the seventh day post-seeding. By day 14, there has been a substantial increase in the diameter of the spheroids of all cell densities. From day 14, 5000 cells spheroids attained plateu and exhibited smaller diameters (112 µm) than 2500 cells spheroids, which had reached 115 µm by that time. A marked increase was observed in 1000 cell spheroids, beginning from day 4 with a mean diameter of 58 µm and reaching 90 µm by day 14. The 2500 cell spheroids maintained their structural integrity and demonstrated the largest mean diameter of 152 µm by day 21. The 5000 cell spheroids, which had a mean diameter of 119 µm, also maintained a relatively intact structure, while the

presence of slight structural degradation was observed. Notably, the 1000 cell spheroids, which demonstrated a significant rise in size by day 21 with a mean diameter of 143 µm, began to disintegrate, exhibiting irregular shapes and cell detachment on the edges. This degradation in the 1000 cell spheroids may be attributed to insufficient cell density to preserve the intact spheroid structure, as well as increased cell death.

4.2.4 Immunofluoresence of Nthy-Ori 3-1 Spheroids

Immunofluorescence was used to examine the structure of 2500 cell Nthy-Ori 3-1 spheroids at days 4, 14, and 21 after seeding. The spheroids were stained with DAPI, a nuclear stain, and Phaloidin, an F-Aktin stain. The DAPI channel images were then processed using Fiji software to count the nuclei using the "3D objects counter" setting. Overall, information about the structure, shape, and the number of nuclei was acquired (Figure 4.6).

(a)

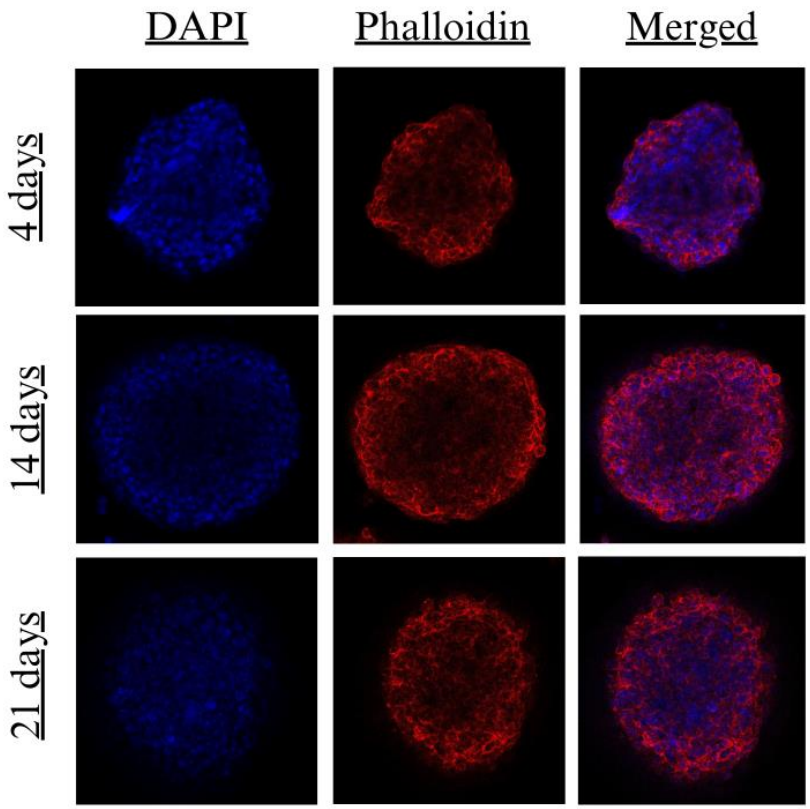

(b)

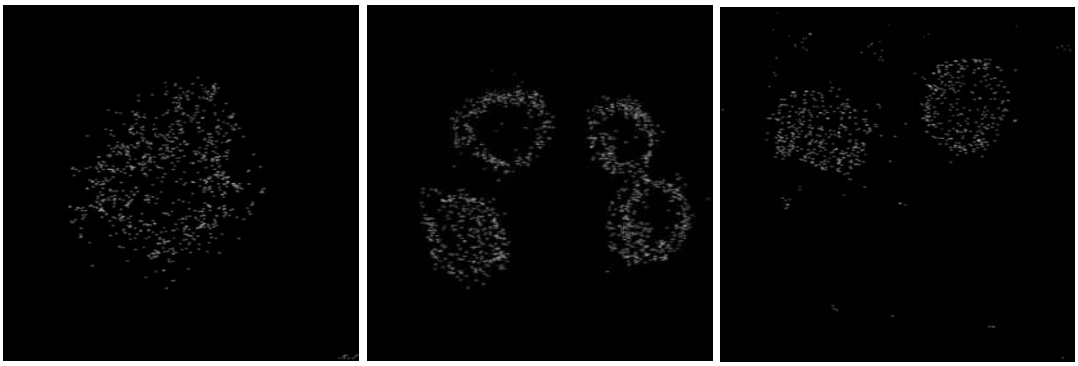

Figure 4.7: Immunofluorescence results:
a. DAPI and Phalloidin staining of 2500 cells Nthy-Ori 3-1 spheroids at 4, 14, and 21 days post-seeding.
b. The images were generated using Fiji's "3D objects counter" setting, with dots representing the nuclei that were counted. The number of objects counted is shown in the right bottom corner of each image. Each condition had only one spheroid's nuclei counted.

On day 4, spheroids were more compact and had less prominent cytoskeletal structure than on days 14 and 21 after seeding. On days 14 and 21, in turn, spheroids appeared larger and structurally intact, with more numerous and condensed nuclei than on day 4. The results are consistent with those shown in Figure 4.6, which illustrates growth patterns and morphological features. In terms of cell count utilizing Fiji software, the number of nuclei counted on the fourth day is slightly higher than on the 14 and 21 days of incubation. This could be attributed to the fact that the nuclei located at the center of the spheroid structure, also known as the necrotic core zone, are more condensed and difficult to separate and count by the software.

4.2.5 Viability Assessment of Nthy-Ori 3-1 Spheroids

Spheroids were evaluated for viability using MTT assays on days 4, 7, 10, 14, and 21 following seeding. Three technical replicates of each condition, 1000, 2500, and 5000, were tested. The viability percentage graph (Figure 4.8a) was created using the

following formula, with 4 days post-seeding spheroids' values serving as the control samples:

$$\text{Cell Viability } (\%) = \frac{Absorbance\ of\ the\ sample - DMSO\ control}{Absorbance\ of\ the\ control\ sample - DMSO\ control} \times 100\%$$

Metabolic activity indicated by viable cells was obtained by graphing incubation time (days) against absorbance at 570nm, which served as another means of representing and statistically analyzing the viability data (Figure 4.8b).

(a)

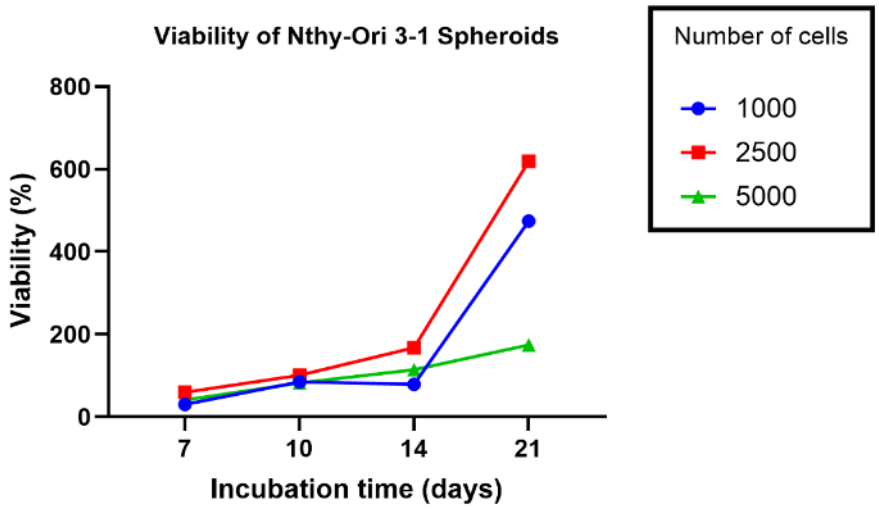

(b)

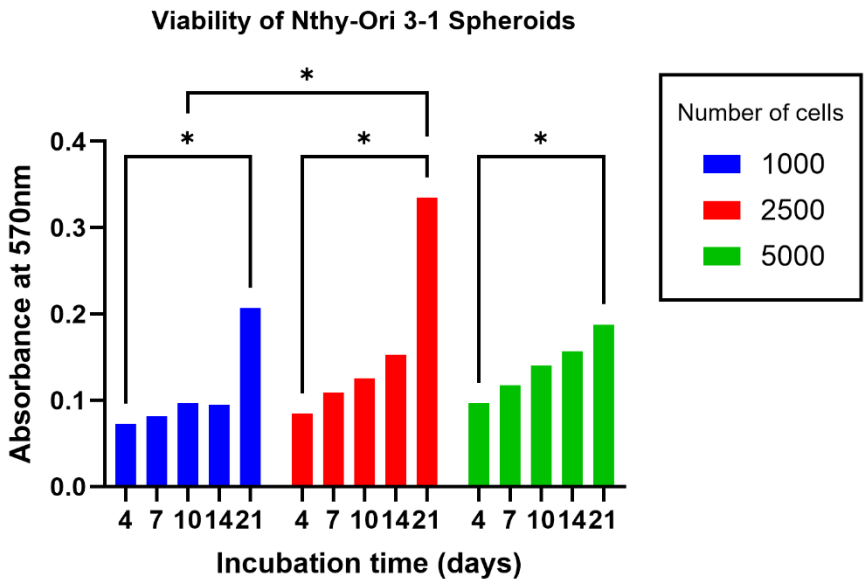

Figure 4.8: Viability Analysis of Nthy-Ori 3-1 spheroids:
(a) Viability Percentage of Nthy-Ori 3-1 spheroids against incubation period (days). (b) Nthy-Ori 3- 1 spheroids viability represented by plotting absorbance at 570 nm against incubation period (days). There is a statistically significant difference ($p \leq 0.05$) between the OD values on days 4 and 21 at all cell densities. In addition, the absorbance rate of 1000 cells spheroids on day 10 is significantly lower ($p \leq 0.05$) than that of 2500 cells spheroids, which have the highest absorbance value. Graphs were created with GraphPad Prism 10.2.3, and 2-way ANOVA (repeated measures) was utilized for statistical analysis.

Despite the differences in representations, both graphs show the same trend and provide a clear picture of the data. From day 4 to 14, viability percentages were high and nearly comparable, with no statistically significant changes ($p \geq 0.05$) between cell densities. However, a gradual increase in viability was seen throughout the incubation period, indicating significant differences between the fourth and final days of incubation. Notably, the absorbance of 2500 cell spheroids is the highest on day 21, and it is significantly different from that of 1000 cell spheroids on day 10 ($p \leq 0.05$).

4.2.6 Determination of Co-culture Ration

Utilizing CFSE labeling, the infiltration patterns of PBMCs were illustrated to aid the identification of the appropriate co-culture ratio and facilitate clear visualization (Figure 4.9).

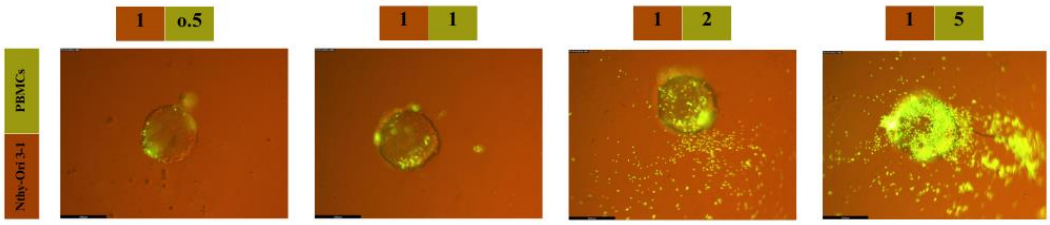

Figure 4.9: The co-culture of Nthy-Ori 3-1 spheroids with CFSE-labelled PBMCs at varying ratios, including 1:0.5, 1:1, 1:2, and 1:5

In the 1:0.5 condition, where 2500 Nthy-Ori 3-1 cells were co-cultured with 1250 PBMCs, the spheroids displayed limited PBMC infiltration, with cells sparsely located along the spheroid's edges. The 1:1 condition showed modest infiltration, with a higher number of PBMCs located closer to the center of the spheroid. Significant infiltration was detected at 1:2 ratio, with a substantial increase in the quantity of PBMCs almost evenly spread throughout the spheroid structure. The 1:5 condition showed the highest infiltration rate, with PBMCs covering the spheroid to the point that it was barely visible. Furthermore, under the 1:2 and 1:5 conditions, an abundance of PBMCs were observed around the spheroid structures.

4.3 Immunophenotyping of 2D and 3D Co-cultures

2500 Nthy-Ori 3-1 cell spheroid co-culture was performed with PBMCs of patients №3 and №8 with TD before and after therapy at a 1:2 ratio. In addition, 2D co-cultures comprised of 500,000 Nthy-Ori 3-1 cells and the same number of PBMCs were also used to facilitate the comparison of observed data. Flow cytometry was utilized to determine how PBMCs affect the viability of Nthy-Ori 3-1 spheroids and 2D monolayers as compared to those without PBMCs. Likewise, immunophenotyping was performed to analyze the probability of immune cell infiltration into spheroid

structures while also identifying the particular types of immune cells that infiltrate the spheroids and at what ratio. Comparisons of immunophenotypes between these patients before and after therapy comprised B cell, T cells and its subtypes (CTLs and THLs), NK cells, and NKT-like cells. This assessment was also carried out on samples of patients without TD and controls to compare the immunophenotypes and correlate with the findings obtained during the immunophenotyping of PBMCs. An appropriate gating strategy for viability assessment and immunophenotyping was implemented (Figure 4.10). The following gating strategy was applied to all samples.

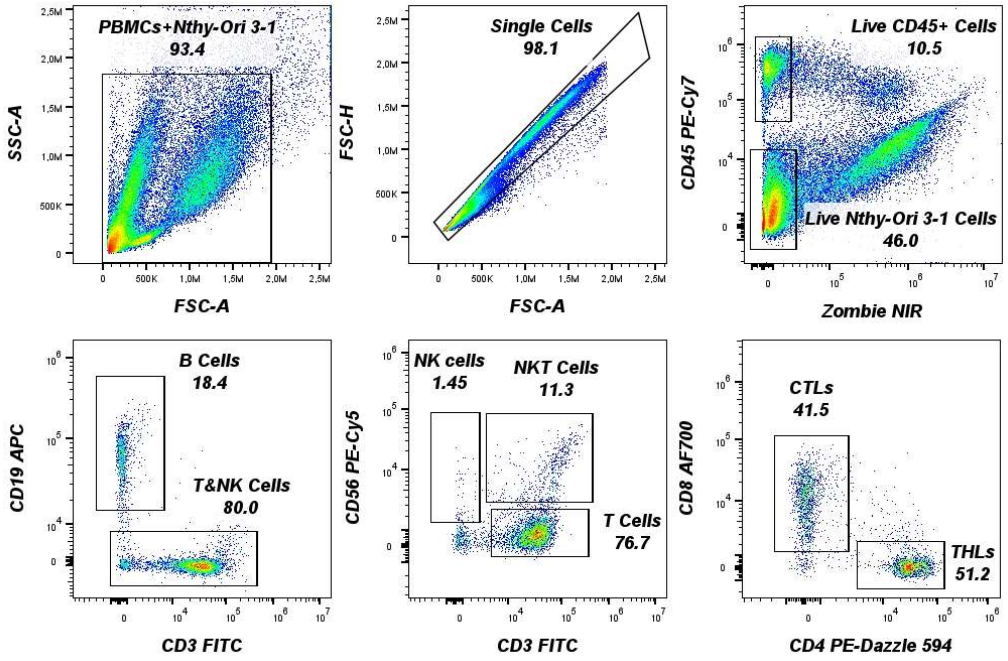

Figure 4.10: Flow cytometry gating strategy for Co-culture experiments.

The total number of Nthy-Ori 3-1 cells and PBMCs was detected by graphing FSC-A versus SSC-A. Doublets were then excluded (FSC-A versus FSC-H), and Nthy-Ori 3-1 cells (Zombie- CD45-) as well as PBMCs (Zombie NIR-CD45+) were gated using a plot of Zombie NIR versus CD45. Following identification of the CD45+ population, B cells (CD19+ CD3-) and T/NK cells (CD19- CD3+) were gated. By plotting CD3 versus CD56 within T and NK cell populations, NK cells (CD56+ CD3-), NKT-like cells (CD3+ CD56+), and T cells (CD3+CD56-) were distinguished. CTLs (CD8+ T cells) and THLs (CD4+ T cells) were further distinguished within the T cell population.

4.3.1 Statistical Analysis

Viability was assessed on 3D and 2D co-cultures containing TD patients' samples before and after therapy. The significant reduction ($p \leq 0.05$) in viability of Nthy-Ori 3-1 cells was observed in 2D co-cultures of patients before and after therapy when compared to Nthy-Ori 3-1 cells without PBMCs, implying that the presence of PBMCs during therapy in a 2D environment has a greater impact on cell viability in terms of cytotoxicity than in a 3D setting, in which the cells appear to be more resilient. Additionally, the viability was evaluated in the presence of PBMCs from patients without TD and control groups to further test the 3D co-culture setting (Figure 4.11).

(a)

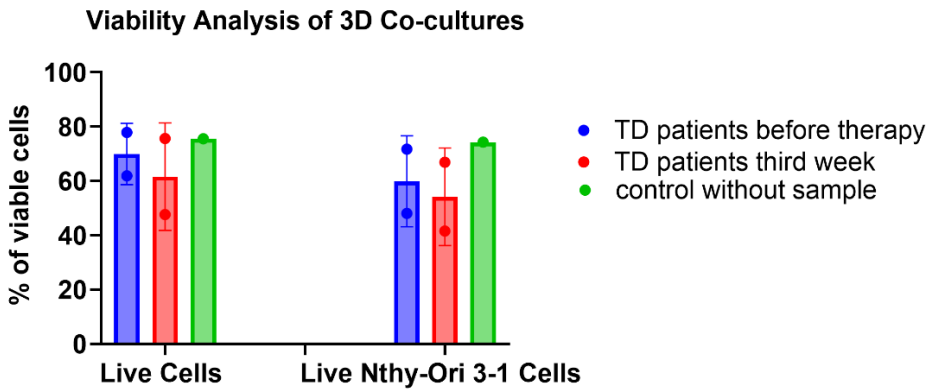

(b)

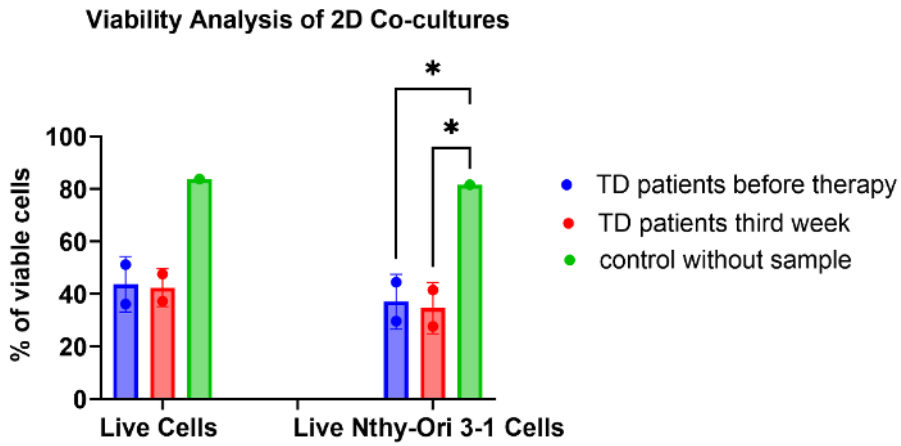

(c)

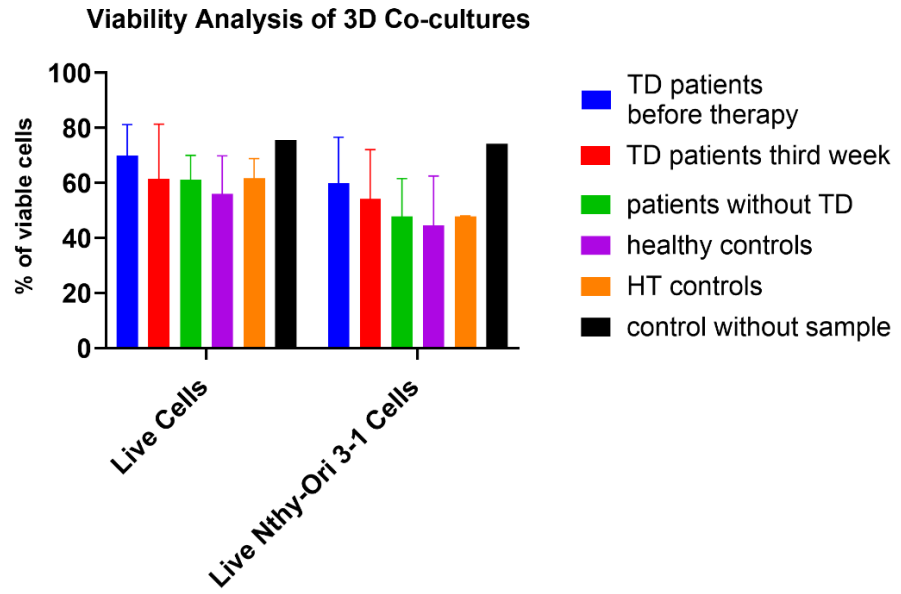

Figure 4.11: Viability analysis of 3D and 2D co-cultures:

(a) In the 3D co-cultures, the viability of Nthy-Ori 3-1 cells showed no statistically significant differences ($p \geq 0.05$) in the presence of PBMCs from patients before and after therapy as compared to the control group without any samples.

(b) In the 2D co-cultures, the viability of Nthy-Ori 3-1 cells significantly decreased ($p \leq 0.05$) in the presence of PBMCs from both patients before and after therapy when compared to control samples.

(c) In the 3D co-cultures, the viability of Nthy-Ori 3-1 cells showed no statistically significant differences ($p \geq 0.05$) in the presence of PBMCs from all study groups as compared to the control group without any samples.

The total number of PBMCs and Nthy-Ori 3-1 cells is referred to as "live cells" in both cultures. When comparing live cells of any of the groups to live Nthy-Ori 3-1 cells, no statistically significant differences ($p \geq 0.05$) were observed. Statistically significant results are marked by asterisks (*). Graphs were created with GraphPad Prism 10.2.3, and 2-way with post-hoc Tukey's test was utilized for statistical analysis.

Following the viability assessment, immune cell infiltration was investigated as part of a prospective 3D model optimization procedure. Immunophenotyping was done on TD patients before and after therapy in both 3D and 2D settings (Figure 4.12). There were not any statistically significant differences ($p \geq 0.05$) in immune cell composition both in 3D and 2D settings, which is consistent with the findings in Figure 4.12a. In addition to TD patients, 3D co-cultures with PBMCs from patients without TD and control samples were also analyzed (Figure 4.12c). Notably, following three weeks of therapy, patients with TD had a significantly greater ($p \leq 0.05$) percentage of infiltrating B cells, which were not detected in PBMC immunophenotyping when referring to Figure 4.12c.

(a)

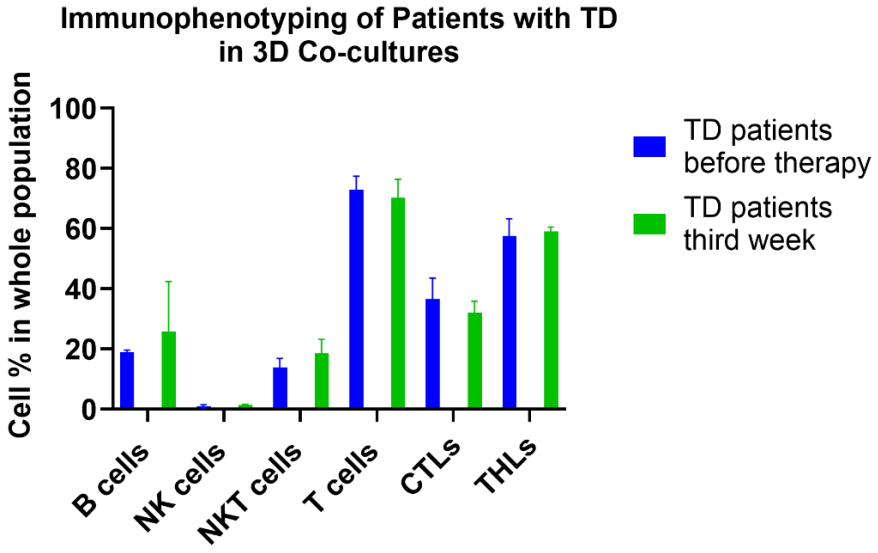

(b)

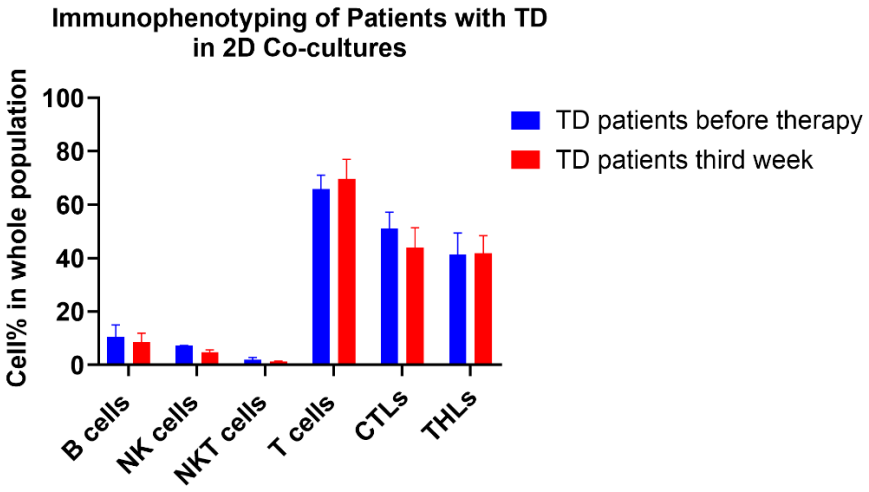

(c)

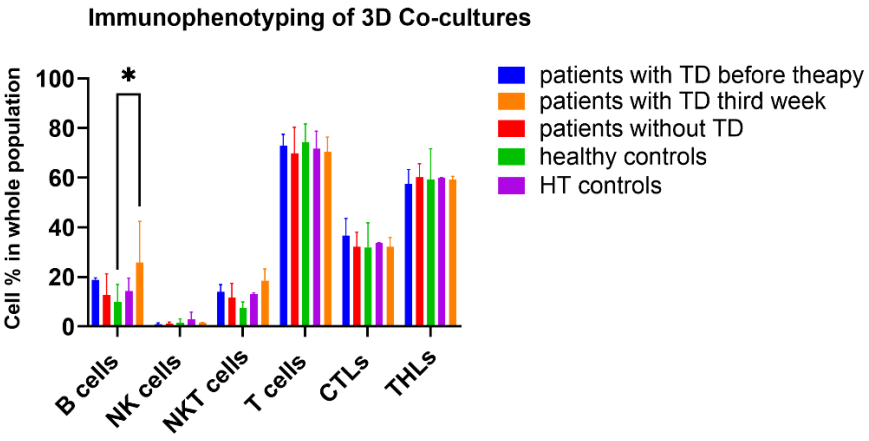

Figure 4.12: Immunophenotyping of 3D and 2D co-cultures:

(a) and (b) Immunophenotyping of Nthy-Ori 3-1 spheroids in co-culture with PBMCs from TD patients before and three weeks after therapy revealed no significant differences ($p \geq 0.05$) in immune cell composition in either 3D or 2D settings. **(c)** Immunophenotyping of 3D co-cultures, consisting of TD patients, patients without TD, healthy controls, and HT controls. In comparison to healthy controls, TD patients exhibited a significantly greater ($p \leq 0.05$) B cell population at the third week following therapy. Statistically significant results are marked by asterisks (*). Graphs were created with GraphPad Prism 10.2.3, and 2-way ANOVA with post-hoc Tukey's test was utilized for statistical analysis.

Chapter 5: **DISCUSSION**

Monoclonal antibodies have emerged as a potent cancer immunotherapy that has the potential to enhance the prognosis for an expanding list of advanced malignancies by blocking immune checkpoint proteins. The prevailing theory is that autoimmune lymphocytic thyroid destruction is the basis of ICI-associated thyroid irAEs, however the exact mechanism is yet unknown. Nevertheless, it is becoming increasingly evident that the underlying mechanism of ICI-associated thyrotoxicosis is might be distinct from typical autoimmunity representation. It is likely an inflammatory, destructive process, as evidenced by the transient thyrotoxic course, which spontaneously remits to either hypothyroidism or euthyroidism. In addition, the clinical presentation of rapid thyroid destruction in ICI-thyroiditis is vastly distinct from the slow, gradual destruction of the thyroid over many years that occurs in Hashimoto's thyroiditis [Lee et al., 2023].

Patients who are receiving ICI typically undergo routine thyroid function monitoring, which includes assessments prior to ICI initiation and during each new cycle of this therapy, due to the fact that these adverse events are largely unpredictable, may occur over a broad time-range, and can be associated with non-specific symptoms. The evaluation of thyroid function is typically not conducted for patients who are receiving conventional chemotherapy or molecularly targeted therapies. As a result, immunotherapy offers a distinctive opportunity to investigate thyroid function in different types of oncology patients [von Itzstein et al., 2022]. In the following study, two of nine patients, Patient №3, a 60-year-old male with Stage IV lung squamous cell carcinoma, and Patient №8, a 44-year-old male with recurrent malignant melanoma, developed TD as early as three weeks after starting treatment. Patient №3 experienced a common thyrotoxicosis phase, which was marked by decreased TSH levels. The following clinical picture, a differential diagnosis for thyroid irAEs, and is associated with low or normal levels of free T4 and free T3, together with low TSH [Chera et al., 2022]. Patient №8, in turn, exhibited a distinctive TD representation, a hormonal dysregulation characterized by elevated fT4 levels and decreased fT3 levels.

Both patients presented with advanced-stage cancers and were treated with Keytruda, a PD-1 inhibitor (patient №3 received it in combination with chemotherapy).

The observed data is consistent with the assertion that TD is more commonly associated with anti-PD-1 therapy, particularly in combination therapy, than with CTLA-4. This is explained by the thyroid's lack of expression of CTLA-4 and the inability of repeated injections of an anti-CTLA-4 antibody to cause hematopoietic cell infiltration [Iwama et al., 2022]. Another significant feature of these patients' clinical data is that both are obese, with a body mass index (BMI) more than 30. A recent meta-analysis found evidence of a link between elevated BMI (overweight-obesity) and an increased risk of irAEs, although additional research is required [Guzman-Prado et al., 2021].

In the following research, three study groups, namely patients before and three weeks after initiation of ICI therapy, healthy controls, and HT patients, were subjected to immunophenotyping by flow cytometry. HT patients representing an autoimmune condition were recruited to elucidate any potential differences in terms of immune cell composition and pro-inflammatory cytokine levels to further make assumptions on underlying mechanisms and identify common traits shared by both conditions. The flow cytometry analysis used a detailed gating strategy to identify various immune cell subsets, including B cells (CD19+ CD3-), NK cells (CD56+ CD3-), NKT-like cells (CD3+ CD56+), T cells (CD3+), CTLs (CD8+ T cells), THLs (CD4+ T cells), and Tregs (CD25+ CD127-). IFN-γ and TNF-α levels were measured within these populations, except for Tregs, to assess immune activation and inflammation.

Statistical analysis initially focused on two TD patients, patients №3 and №8. In these cases, no statistically significant differences were observed in immune cell percentages or cytokine levels (IFN-γ and TNF-α) before and three weeks after therapy. This lack of significance mainly suggests the limited sample size, reducing the power of statistical analysis, and also suggests that the development of TD in these patients may not be directly associated with major shifts in immune cell composition or cytokine expression at the time points examined. Expanding the analysis to all patient samples (n=8), the study found no significant changes in the overall composition of immune cell subsets between pre-therapy and post-therapy samples. However, significant increases in IFN-γ producing CTLs and NK cells, alongside a significant rise in TNF-α producing B cells after three weeks of therapy. Although the overall percentage of NKT-like cells releasing TNF-α did not change significantly, the expression levels measured by mean

fluorescence intensity (MFI) were significantly greater in the third week of therapy. This could represent increased functional activity of these cells, implying a more powerful inflammatory response within this fraction. NKT-like cells have been discovered for their ability to generate substantial quantities of TNF-α in response to a pro-inflammatory environment, which can be attributed to the activation of immune cells in order to combat cancer after the administration of a PD-1 blocker [Almeida et al., 2023].

A comparison of immune cell composition across all groups, including healthy controls (n=6) and HT controls (n=3), showed no significant changes. HT controls had significantly greater levels and intensities of IFN-γ and TNF-α producing pro-inflammatory immune cells than both patients and healthy controls. In this control group, TNF-α expression was considerably higher in CTLs and NK cells compared to healthy individuals, indicating a heightened inflammatory response. HT is primarily a Th1 immune response, and the production of Fas/FasL in response to pro-inflammatory cytokines such as IFN-γ and TNF-α triggers thyroid cell death (Mikoś et al., 2014). This pattern was therefore anticipated and acted as a counterbalance to immunological dysregulation. Notably, patients' TNF-α producing B cells increased significantly following three weeks of ICI therapy, which is consistent with results in the HT control group. B lymphocytes, traditionally known for their role in producing antibodies, also have the capacity to produce cytokines, which can modulate immune responses. The effector functions of these cytokine-producing B cells are indeed context-dependent and heavily influenced by the surrounding cytokine milieu [de Gruijter et al., 2022].

There is a lack of research on immunophenotyping patients with ICI-induced irAEs, particularly thyroid complications. According to Kotwal et al., (2020), the first thorough immunophenotyping of patients with ICI-induced thyroiditis was carried out in both the thyroid and the blood. Patients with ICI-induced thyroiditis (n = 8) had higher intra-thyroidal CD3+ and CD8+ T lymphocytes, but there was no discernible difference in the blood (n =13) when compared to healthy volunteers (n = 44). B lymphocyte counts were higher in the blood and thyroid than in controls. Conversely, the blood exhibited an increase in NK cells and intermediate monocytes, while the thyroid did not exhibit a significant difference from the controls [Kotwal et al., 2022].

Furthermore, it has been shown that the presence of CD8+ T cells, CD4+ T cells, and activated B cells can be used to predict the effectiveness of ICI therapy. The reduction of these cells greatly diminished the effectiveness of the treatment [Hollern et al., 2019]. None of these modifications in the immune cell composition were observed in this investigation. To further validate the reported findings, future research should concentrate on expanding the sample size.

ICI triggers an anti-tumor cellular and humoral response, implying a pro-inflammatory shift in the release of cytokines, including IL-6, IFNγ, and other inflammatory cytokines. The cytokine profile is not limited to the tumor milieu and has a systemic effect, even if it is believed to particularly influence tumor micro-environment. Greater local inflammatory responses against tumors are related to stronger systemic effects that lead to extra-tumor inflammatory responses that may have a self-reactive effect [Bracamonte-Baran and Kim, 2024]. In addition, as demonstrated in the case of IFN-α-induced thyroiditis, inflammatory cytokines may directly affect thyrocytes, thereby contributing to the accelerated destruction of the thyroid [Lee et al., 2023].

To the best of our knowledge, this is the first study to compare the levels of immune cells producing IFN-γ and TNF-α in patients to those found in HT patients and control subjects, both before to ICI therapy and as early as three weeks later in the context of ICI-induced TD. A proposed mechanism of elevated inflammation levels in these patients is correlated with increased IFN-γ levels of CTLs and NK cell subsets, TNF-α producing B cells, and elevated expression of TNF-α in NKT-like cells after three weeks of therapy, even though no correlation was found in TD patients given the limited sample size. Furthermore, a statistically significant rise in TNF-α producing B cells compared to healthy controls was detected when comparing all study groups. By revealing a significant rise in the cytokine levels of several immune cell subsets, the HT group demonstrated a more profound inflammatory response when compared to the patient group. The question of whether PD-1 inhibition triggers a B cell-mediated humoral autoimmune response remains ambiguous. Despite TD manifestation, several case reports showed that patients receiving ICIs had negative auto-antibodies. It was also proposed that the release of thyroid antigens during the course of destructive

thyroiditis caused humoral immunity to produce thyroid auto-antibodies [Zhan et al., 2021]. Thus, assessing thyroid autoantibody levels before and during ICI therapy is critical, and one of the study's limitations.

Although not as extensively manifested as TD, there is a wide range of ICI-induced irAEs that share underlying mechanisms that necessitate further investigation. The comprehension of the mechanisms that underlie ICI-induced thyroiditis may also provide insight into other irAEs. For example, a study on ICI-induced arthritis comprehensively characterized a variety of cytokines and discovered elevated serum levels of Th1-associated cytokines, including IL-12, TNF-α, and IFN-γ. The *ifng* gene, which encodes IFN-γ, was found to be the most abundantly expressed gene in the gene expression analysis, particularly in NK cells, NK-T cells, and specific T cell subclusters. Additionally, genes that encode TNF-α, granzyme B, granzyme K, granzyme H, granulysin, and GM-CSF, which are correlated with inflammatory responses, were also highly expressed [Kim et al., 2022]. This indicates a robust inflammatory response associated with ICI therapy, which is in accordance with the observed data.

The lack of power resulting from the small number of patients is a significant limitation of the immunophenotyping that was conducted. This may account for the fact that certain findings did not qualify for statistical significance. Additionally, immunophenotyping data interpretation presents certain challenges. Due to the great degree of immunological heterogeneity in humans, it is yet unclear how previous therapies, such chemotherapy, affect their response to ICI therapy. The development of ICI-induced irAEs, particularly TD, is further restricted by the limited timeframe. By increasing the number of patients and extending the observation period, the current study will be enhanced to acquire more comprehensive data. Despite the aforementioned limitations, this study has strengths in including the HT control group and defining the first potential differences in immune cell makeup and inflammatory responses in patients receiving ICI therapy, which may be accounted for predictive biomarkers in the longitudinal perspective.

The second in-vitro modeling component of this research was inspired by the Saraiva et al., (2020) study which worked on the establishment of a 3D co-culture with

the MDA-MB-231 breast cancer cell line and patient-derived PBMCs. The tumor cells' viability was evaluated using flow cytometry in the presence of patient-derived PBMCs, either with or without prior stimulation. Remarkably, the majority of breast cancer patients' PBMCs were found to decrease the tumor cells' viability. The potential application of this platform for personalized immune-based drug screening was suggested, with results accessible after a maximum of 10 days of culture [Saraiva et al., 2020]. In the context of the present study, the viability of Nthy-Ori 3-1 cell line spheroids in the presence of TD patients' PBMCs was also evaluated, as the destruction of thyroid follicular cells is marked in TD patients following ICI therapy. The justified use of the Nthy-Ori 3-1 cell line was due to its origins in follicular epithelial thyroid cells. To further clarify the potential of using the following 3D co-culture model in immunophenotyping and to demonstrate what types of immune cells and at what rate are infiltrating, flow cytometry was also performed as a means of attempting to immunophenotype the TD patients before and three weeks after the initiation of ICI therapy along with healthy and HT control groups. To the best of our knowledge, this is the first 3D co-culture model established and optimized for the Nthy-Ori 3-1 cell line and patients' PBMCs.

The model development process began with optimizing technical protocols for producing Nthy-Ori 3-1 spheroids. There are several ways to generate 3D spheroids, including applying microfluidic devices, hanging drop technique, matrix-on-top/embedded, and ultra-low attachment plates. The present study used the matrix-on-top approach using agarose coating methodology which is cost-effective, does not necessitate specialized equipment, has a high level of reproducibility, and is capable of large-scale production. A variety of cell densities were tested to determine the optimal seeding cell number. For instance, the initial concentration of 1000 cells was employed in the study conducted by Oh et al., (2020) and the complete formation of Nthy-Ori 3-1 spheroids was observed 10 days following incubation [Oh et al., 2022]. The lack of information regarding the optimal seeding number for this particular cell line provided the justification for examining 1000, 2500, and 5000 cells. The spheroids' highest growth and structural stability were observed at an initial concentration of 2500 cells. On the 21 day of incubation, the maximum diameter of 142 μm was attained with this cell density. However, the initial signs of structural disintegration began to emerge,

although these appeared not as severe as the ones observed with 1000 cell spheroids. As with 1000 cell spheroids, after 21 days of incubation, there was a complete loss of structural integrity, resulting in considerable cell detachment. With a maximum diameter of 117 μm, 5000 cell spheroids appeared larger at first but achieve their plateu by day 14. Higher amounts of apoptotic markers are found in larger spheroids, which may be related to limitations in nutrition and transport. With resources readily available, smaller spheroids displayed enhanced metabolic activity and proliferation [Griffin et al., 2022].

Depending on the type of cell, different 3D models take varying periods of time to completely form. In accordance to certain investigations, day 7 is the optimum time for manipulating the spheroids, as is the case with primary human hepatocyte spheroids and human mesenchymal stem cell spheroids. Other studies have shown that the very first day of development may be sufficient for tumor cell aggregates, such as glioma spheroids [Brochado et al., 2023]. In the case of Nthy-Ori 3-1 cell line, the spheroids were uniform and stable from day 4. Immunofluorescence imaging revealed that the spheroids were well organized and intact during a 21-day incubation period. In addition to observing the morphological arrangement of spheroids, immunofluorescence imaging was utilized to attempt the quantification of the number of cells, specifically counting their nuclei. The counts that the Fiji "3D objects counter" reported were actually lower than the original seeding numbers. In addition, spheroid incubation for 4 days revealed more "objects" identified than spheroid incubation for 14 and 21 days. The cells' strong cell-to-cell adhesions and production of extracellular matrix (ECM) within the spheroid, which creates a gradient of nutrients, oxygen, and signaling molecules, may be the cause of these observations [Higashi et al., 2022]. This gradient results in spheroids having a necrotic core, a hypoxic inner layer of quiescent cells, and an outer layer of proliferating cells that is well-oxygenated. Cells may vary in size while culture; the cells inside a spheroid are smaller than the cells outside [Białkowska et al., 2020]. Thereby, nuclei in a necrotic region, appear denser and may be harder for the program to separate, resulting in fewer objects being detected. This suggests that as the spheroid ages, the necrotic core appears to expand in size. Spheroids formed shortly after formation can be manipulated in the subsequent experiments to reduce the amount of dead cells in the structure's core.

When the spheroids had fully formed, all three densities were evaluated for viability. Day 4, 7, 10, 14, and 21 were used to investigate the viability dynamics using the MTT assay. The mono-tetrazolium salt known as the MTT reagent (3-(4,5-dimethylthiazol-2-yl)-2,5-diphenyl-2H-tetrazolium bromide) is composed of a positively charged quaternary tetrazole ring core that is surrounded by three aromatic rings, which include two phenyl moieties and one thiazolyl ring. The core tetrazole ring is disrupted upon reduction of MTT, and formazan, a violet-blue water-insoluble molecule, is formed. Due to its lipophilic nature and positive charge, the MTT reagent is capable of passing through both the cell membrane and the inner membrane of the mitochondria of live cells which then convert it to formazan [Ghasemi et al., 2021]. The viability analysis clearly illustrated the trend of a direct correlation between the viability percentage or absorbance values and the size of Nthy-Ori 3-1 spheroids. Given that the physical proximity of cells to one another can change intercellular communication and therefore modify the metabolic processes of the cells, the observed rise in absorbance could potentially be the result of an increase in cell density. In simpler terms, the nature of intercellular signaling and the enzymatic activity of each cell may be altered by a higher cell density, which in turn affects the amount of formazan produced [Ward and Thompson, 2012].

MTT assay may exhibit a lack of sensitivity in the context of the Nthy-Ori 3-1 spheroids. At present, the literature showcases several MTT-based studies that claim to be effective in viability assessments, including 3D cultures and, more significantly, in drug cytotoxicity analyses. Nevertheless, research also indicates that colorimetric tests utilizing the reduction in tetrazolium are not suitable for use in 3D models due to the possibility of dye absorption and kinetic diffusion being impacted by the dense matrix, therefore affecting absorption readings [Brochado et al., 2023]. As an alternative to the traditional MTT assay, the CellTiter-Glo 3D Cell Viability Assay quantifies ATP, a marker of metabolically active cells. Future research should compare the results of this assay, which is widely used in 3D cultures, to those obtained from MTT in the case of Nthy-Ori 3-1 spheroids. The assay is distinguished by its high sensitivity, as it operates by lysing cells within the 3D structure to release ATP. This ATP subsequently reacts with luciferase and luciferin in the reagent, resulting in a luminescent signal. This light's

intensity is directly correlated with ATP levels and, consequently, with the quantity of living cells [Kijanska and Kelm, 2016].

Given the viability results, immunofluorecsence data and the optimum cell number for seeding, it was determined that the subsequent 3D co-culture model development would comprise 2500 cell Nthy-Ori 3-1 spheroids on the fourth day post-incubation. The final evaluation prior to performing a co-culture with the patient and control PBMCs included defining a co-culture ratio and visual representation. 2500 cell spheroids were co-cultured with control sample PBMCs at ratios of 1:0.5, 1:1, 1:2, and 1:5. At 1:1 and 1:0.5 ratios, the amount of PBMCs was comparable, with modest infiltration rates and uneven distribution throughout the spheroid structure. The spheroid structure was nearly invisible in the 1:5 ratio due to the extremely high number of PBMCs compared to Nthy-Ori 3-1 cells, whereas in the 1:2 ratio, PBMCs were evenly and highly distributed throughout the spheroid structure, making it the preferred option. Likewise, the research conducted by Yakavets et al., (2020) revealed that high co-culture ratios of MCF-7 spheroids with fibroblasts were associated with a high likelihood of spheroids dissociating, rendering co-culture ratios in which only fibroblasts were visible unfavorable for subsequent analyses [Yakavets et al., 2020]. Considering all the information, a 1:2 ratio of PBMCs for 2500 cell Nthy-Ori 3-1 spheroids was selected for flow cytometry analyses since higher co-culture ratios would alter the spheroids' characteristics, but lower ratios might not be sufficient for analysis.

Viability assessment and immunophenotyping using flow cytometry on Nthy-Ori 3-1 spheroid co-cultures with PBMCs were intended solely as a case study to optimize the protocols and identify any potential improvements that need to be taken into account when applied to a larger sample size and as part of the initial stages of in-vitro model development. Nthy-Ori 3-1 spheroids exhibited no statistically significant differences in viability in the presence of TD patients' PBMCs (Patients №3 and №8) before therapy and three weeks afterward compared to a control group without the sample. When all groups, including healthy and HT controls, patients without TD, and healthy controls, were analyzed collectively, the same results were obtained. This may indicate that the presence of patients' immune cells, which are believed to play a role in thyroid cell

destruction, did not reduce the viability of Nthy-Ori 3-1 cells; yet, further validation of the obtained findings requires larger sample size research.

In order to identify any potential discrepancies between the 3D and 2D contexts, a viability testing on 2D co-cultures was additionally conducted for experimental purposes. Noteworthy, the viability of thyroid cells in the presence of both patients before therapy and after the third week of therapy dropped. Compared to conventional monolayer (2D) cell culture, in which cells are grown affixed to plastic, 3D cell culture more closely resemble the natural in vivo environment. The proliferation, differentiation, apoptosis, gene and protein expression, and numerous other cellular processes can be influenced by the aberrant cell morphology in the 2D cell culture [Liu et al., 2022]. Nevertheless, the role of the ECM-like microenvironment in 3D cultures on the cells is still uncertain. There is still debate over the extent that the behavior and metabolism of the cells change in 3D settings, and research comparing traditional 2D and 3D models is currently in progress [Edmondson et al., 2014]. Although it is difficult to draw conclusions about the relationship between thyroid cell viability and TD patient samples based on this data, it is clear that 2D and 3D cell cultures represent different biological information, necessitating further research.

The immune cell infiltration patterns of B cells (CD19+ CD3-), NK cells (CD56+ CD3-), NKT-like cells (CD3+ CD56+), T cells (CD3+), CTLs (CD8+ T cells), and THLs (CD4+ T cells) in TD patients before and three weeks after therapy were observed through immunophenotyping of 3D co-cultures. It is important to mention that the entire media containing floating non-infiltrating PBMCs was removed during the sample preparation for flow cytometry in order to exclude those cells that did not infiltrate the spheroids. In addition, control groups and patients without TD were also included in the analysis to explore if the findings of PBMCs immunophenotyping could be correlated. In the case of TD patients, no significant differences were observed, which is consistent with the data observed for PBMCs analysis of these patients, given the limited sample size. In contrast to healthy individuals, patients' B cell populations increased significantly after three weeks of therapy, a difference that was not observed across all research groups. B cells have been shown to play a role in other types of thyroiditis, such as Hashimoto's thyroiditis, although their participation in ICI-induced

irAE tends to be less significant. Studies suggest that the thyroid immune infiltrates in ICI-thyroiditis are primarily composed of T cells, with a small number of B cells present [Lechner et al., 2021]. Although the resulting findings illustrate the data that must be considered, it is crucial to emphasize that this is the first study to attempt immunophenotyping of patients receiving ICI therapy in 3D context. Increasing the sample size and observation durations may aid in determining the reliability of the patterns observed. {Korbecki, 2020 #121}

The reliance on an allogeneic system, wherein the Nthy-Ori 3-1 cell line's MHC molecules do not match the TCR of patient-derived T cells, is the principal limitation of this investigation. While T cell alloreactivity is highlighted by this approach, the precise interactions that would take place in an autologous system are not fully replicated. The difficulties in collecting and keeping viable patient-specific cells, along with the variability that can make standardization and reproducibility difficult, make developing an autologous system highly challenging. As each element of the allogeneic model is optimized, the shift towards an autologous system, where immune cells and target tissues are completely compatible, becomes increasingly feasible.

This progression could lead to the creation of highly individualized models that are invaluable in studying severe cases, where detailed insights into a patient’s unique immune interactions are essential [Saraiva et al., 2020].

This study is innovative in that it is the first to develop an in vitro model specifically designed to study ICI-related TD, a condition that resembles autoimmune diseases but also possesses unique immune mechanisms, that require further elucidation. Despite the drawbacks of the system, alloreactive T cells provide useful preliminary insights that can be refined in future autologous models. With its well-described protocols, this study acts as a significant methodological guide that might be used as a template to study other autoimmune thyroid disorders not limited to ICI-induced TD. Furthermore, incorporating sophisticated techniques like Western blotting, qPCR, and ELISA could considerably improve the model's efficiency by offering deeper insights into the underlying molecular pathways.

Chapter 6: **CONCLUSION**

1. Two out of nine patients developed ICI-induced TD within three weeks of treatment with a PD-1 inhibitor. One patient showed hormonal dysregulation with elevated fT4 and decreased fT3 levels, while the other experienced a typical thyrotoxicosis phase with decreased TSH levels. No significant changes were observed in immune cell percentages or IFN-γ and TNF-α levels before and after therapy, given a limited sample size.
2. When the analysis was extended to include all patient samples, significant increases were observed in IFN-γ producing CTLs and NK cells, as well as in TNF-α producing B cells after three weeks of therapy. Additionally, there was an increase in TNF-α expression levels in NKT-like cells. When comparing all study groups, the increase was specifically noted in TNF-α producing B cells when compared to pre-therapy levels and healthy controls.
3. The findings observed might be due to the activation of immune cells, leading to the production of pro-inflammatory cytokines aimed at combating tumor cells. However, these results could also serve as predictive biomarkers for the development of irAEs and treatment outcomes, offering insights into the underlying mechanisms of irAEs, including ICI-induced TD.
4. Future immunophenotyping studies should prioritize expanding the sample size, extending observation periods, and evaluating thyroid autoantibody levels to achieve more consistent results.
5. The development of the 3D co-culture model was initiated to specifically study the ICI-induced TD given it unclear mechanisms, and began with the optimization of technical protocols, which included monitoring spheroid growth and morphology, conducting viability tests, and visualizing PBMC infiltration.
6. The key findings from the 3D co-culture model development revealed that Nthy-Ori 3-1 spheroids fully formed by the fourth day when seeded with 2,500 cells, which was identified as the optimal seeding number, resulting in higher viability, growth, and structural integrity. The co-culture ratio for Nthy-Ori 3-1 spheroids with PBMCs at this cell number was determined to be 1:2, as this ratio provided high and even infiltration within the spheroid structures. However,

some experimental approaches still require further optimization, particularly in terms of viability assessment.

7. Downstream testing of the 3D co-cultures included viability analysis and immunophenotyping through flow cytometry. In the context of ICI-induced TD, no statistically significant differences were found in the viability of Nthy-Ori 3-1 cells between TD patients and control groups in the 3D setting. However, viability significantly decreased in the 2D setting, which may be due to the more physiologically relevant nature of the 3D environment. These findings highlight the distinct biological information provided by 2D and 3D cell cultures, underscoring the need for further research with an expanded sample size.
8. Immunophenotyping results on 3D co-cultures indicated no statistically significant differences among TD patients, which is consistent with findings from PBMC analysis. When compared to healthy individuals, patients experienced a significant increase in B cell populations after three weeks of therapy. Expanding the sample size and extending observation periods could help verify the reliability of the observed patterns.
9. The primary limitation of this study lies in its reliance on an allogeneic system. While challenging due to variability and difficulties in collecting viable patient-specific cells, the development of an autologous system could provide highly individualized models essential for studying severe cases. Despite these challenges, this study is pioneering as the first to create an in vitro model specifically for investigating ICI-related TD, offering preliminary insights and serving as a methodological guide for future thyroid research.

Chapter 7: **BIBLIOGRAPHY**

[Abbas et al., 2017] Abbas, A.K., Lichtman, A.H., and Pillai, S. (2017). *Cellular and Molecular Immunology*. Elsevier.

[Almeida et al., 2023] Almeida, J.S., Casanova, J.M., Santos-Rosa, M., Tarazona, R., Solana, R., and Rodrigues-Santos, P. (2023). Natural killer T-like cells: Immunobiology and role in disease. *International Journal of Molecular Sciences*, 24(3), 2743. https://doi.org/10.3390/ijms24032743. PMID: 36769064; PMCID: PMC9917533.

[Althwaiqeb and Bordoni, 2023] Althwaiqeb, S.A., and Bordoni, B. (2023). Histology, B cell lymphocyte. In: StatPearls [Internet]. Treasure Island (FL): StatPearls Publishing; 2024 Jan-. Available from: https://www.ncbi.nlm.nih.gov/books/NBK560905/.

[Alturki, 2023] Alturki, N.A. (2023). Review of the immune checkpoint inhibitors in the context of cancer treatment. *Journal of Clinical Medicine*, 12(13), 4301. https://doi.org/10.3390/jcm12134301. PMID: 37445336; PMCID: PMC10342855.

[Andreeva et al., 2023] Andreeva, V.D., Ehlers, H., R. C., and A.K. et al. (2023). Combining nitric oxide and calcium sensing for the detection of endothelial dysfunction. *Communications Chemistry*, 6, 179. https://doi.org/10.1038/s42004-023-00973-8.

[Antonia et al. 2017] Antonia, S.J., Villegas, A., Daniel, D., Vicente, D., Murakami, S., Hui, R., Yokoi, T., Chiappori, A., Lee, K.H., de Wit, M., Cho, B.C., Bourhaba, M., Quantin, X., Tokito, T., Mekhail, T., Planchard, D., Kim, Y.C., Karapetis, C.S., Hiret, S., Ostoros, G., Kubota, K., Gray, J.E., Paz-Ares, L., de Castro Carpeño, J., Wadsworth, C., Melillo, G., Jiang, H., Huang, Y., Dennis, P.A., and Özgüroğlu, M.; PACIFIC Investigators. (2017). Durvalumab after Chemoradiotherapy in Stage III Non-Small-Cell Lung Cancer. *N Engl J Med*, 377(20), 1919-1929. https://doi.org/10.1056/NEJMoa1709937. Epub 2017 Sep 8. PMID: 28885881.

[Białkowska et al., 2020] Białkowska, K., Komorowski, P., Bryszewska, M., & Miłowska, K. (2020). Spheroids as a Type of Three-Dimensional Cell Cultures—Examples of Methods of Preparation and the Most Important Application. *Int J Mol Sci*, 21(17), 6225. https://doi.org/10.3390/ijms21176225.

[Bracamonte-Baran and Kim, 2024] Bracamonte-Baran, W., & Kim, S.T. (2024). The Current and Future of Biomarkers of Immune Related Adverse Events. *Rheum Dis Clin North Am*, 50(2), 201-227. https://doi.org/10.1016/j.rdc.2024.01.004.

[Brahmer et al. 2015] Brahmer, J., Reckamp, K.L., Baas, P., Crinò, L., Eberhardt, W.E., Poddubskaya, E., Antonia, S., Pluzanski, A., Vokes, E.E., Holgado, E., Waterhouse, D., Ready, N., Gainor, J., Arén Frontera, O., Havel, L., Steins, M., Garassino, M.C., Aerts, J.G., Domine, M., Paz-Ares, L., Reck, M., Baudelet, C., Harbison, C.T., Lestini, B., and Spigel, D.R. (2015). Nivolumab versus Docetaxel in Advanced Squamous-Cell Non-Small-Cell Lung Cancer. *N Engl J Med*, 373(2), 123-135. https://doi.org/10.1056/NEJMoa1504627. PMID: 26028407; PMCID: PMC4681400.

[Brochado et al., 2023] Brochado, A.C.B., Silva, D.C., Silva, J.C.d., Lowenstein, A., Gameiro, V.S., Mavropoulos, E., Mourão, C.F., & Alves, G.G. (2023). Characterization and Applicability of a Bone Spheroid Model for the Evaluation of Cytocompatibility of Bone Substitutes. *Appl. Sci.*, 13, 1602. https://doi.org/10.3390/app13031602.

[Cai et al., 2022] Cai, T., Du, P., Suo, L., Jiang, X., Qin, Q., Song, R., Yang, X., Jiang, Y., and Zhang, J.A. (2022). High iodine promotes autoimmune thyroid disease by activating hexokinase 3 and inducing polarization of macrophages towards M1. *Frontiers in Immunology*, 13, 1009932. https://doi.org/10.3389/fimmu.2022.1009932. PMID: 36325332; PMCID: PMC9618622.

[Cardona et al. 2023] Cardona, Z., Sosman, J.A., Chandra, S., and Huang, W. (2023). Endocrine side effects of immune checkpoint inhibitors. *Frontiers in Endocrinology (Lausanne)*, 14, 1157805.

https://doi.org/10.3389/fendo.2023.1157805. PMID: 37251665; PMCID: PMC10210589.

[Chalan et al., 2018] Chalan, P., Di Dalmazi, G., Pani, F., et al. (2018). Thyroid dysfunctions secondary to cancer immunotherapy. *Journal of Endocrinological Investigation*, 41, 625–638. https://doi.org/10.1007/s40618-017-0778-8.

[Chera et al. 2022] Chera, A., Stancu, A.L., and Bucur, O. (2022). Thyroid-related adverse events induced by immune checkpoint inhibitors. *Frontiers in Endocrinology (Lausanne)*, 13, 1010279. https://doi.org/10.3389/fendo.2022.1010279. PMID: 36204105; PMCID: PMC9530140.

[Chye et al. 2022] Chye, A., Allen, I., Barnet, M., and Burnett, D.L. (2022). Insights into the host contribution of endocrine-associated immune-related adverse events to immune checkpoint inhibition therapy. *Frontiers in Oncology*, 12, 894015. https://doi.org/10.3389/fonc.2022.894015. PMID: 35912205; PMCID: PMC9329613.

[de Filette et al. 2022] de Filette, J.M.K., André, S., De Mey, L., et al. (2022). Durvalumab-induced thyroiditis in a patient with non-small cell lung carcinoma: A case report and review of pathogenic mechanisms. *BMC Endocrine Disorders*, 22, 291. https://doi.org/10.1186/s12902-022-01190-5.

[de Gruijter et al., 2022] de Gruijter, N.M., Jebson, B., & Rosser, E.C. (2022). Cytokine production by human B cells: role in health and autoimmune disease. *Clin Exp Immunol.*, 210(3), 253-262. https://doi.org/10.1093/cei/uxac090.

[Deligiannis et al. 2021] Deligiannis, N.G., Sosa, S., Danilowicz, K., and Rizzo, L.F.L. (2021). Endocrine dysfunction induced by immune checkpoint inhibitors. *Medicina*, 81, 269–278.

[Deligiorgi et al. 2021] Deligiorgi, M.V., Sagredou, S., Vakkas, L., and Trafalis, D.T. (2021). The continuum of thyroid disorders related to immune checkpoint

inhibitors: Still many pending queries. *Cancers*, 13(21), 5277. https://doi.org/10.3390/cancers13215277.

[Dobosz and Dzieciątkowski, 2019] Dobosz, P., and Dzieciątkowski, T. (2019). The intriguing history of cancer immunotherapy. *Frontiers in Immunology*, 10, 2965. https://doi.org/10.3389/fimmu.2019.02965. PMID: 31921205; PMCID: PMC6928196.

[Dutta et al., 2023] Dutta, S., Ganguly, A., Chatterjee, K., Spada, S., and Mukherjee, S. (2023). Targets of immune escape mechanisms in cancer: Basis for development and evolution of cancer immune checkpoint inhibitors. *Biology*, 12, 218. https://doi.org/10.3390/biology12020218.

[Edmondson et al., 2014] Edmondson, R., Broglie, J.J., Adcock, A.F., & Yang, L. (2014). Three-dimensional cell culture systems and their applications in drug discovery and cell-based biosensors. *Assay Drug Dev Technol.*, 12(4), 207-218. https://doi.org/10.1089/adt.2014.573.

[Fabien et al., 1994] Fabien, N., Fusco, A., Santoro, M., Barbier, Y., Dubois, P.M., and Paulin, C. (1994). Description of a human papillary thyroid carcinoma cell line. Morphologic study and expression of tumoral markers. *Cancer*, 73(8), 2206-2212. https://doi.org/10.1002/1097-0142(19940415)73:8<2206::aid-cncr2820730828>3.0.co;2-m. PMID: 8156527.

[Ghasemi et al., 2021] Ghasemi, M., Turnbull, T., Sebastian, S., & Kempson, I. (2021). The MTT Assay: Utility, Limitations, Pitfalls, and Interpretation in Bulk and Single-Cell Analysis. *Int J Mol Sci*, 22(23), 12827. https://doi.org/10.3390/ijms222312827.

[González-Navajas et al., 2021] González-Navajas, J.M., Fan, D.D., Yang, S., Yang, F.M., Lozano-Ruiz, B., Shen, L., and Lee, J. (2021). The impact of Tregs on the anticancer immunity and the efficacy of immune checkpoint inhibitor therapies. *Frontiers in Immunology*, 12, 625783. https://doi.org/10.3389/fimmu.2021.625783. PMID: 33717139; PMCID: PMC7952426.

[Griffin et al., 2022] Griffin, K.H., Fok, S.W., & Kent Leach, J. (2022). Strategies to capitalize on cell spheroid therapeutic potential for tissue repair and disease modeling. *NPJ Regen Med*, 7(1), 70. https://doi.org/10.1038/s41536-022-00266-z.

[Guzman-Prado et al., 2021] Guzman-Prado, Y., Ben Shimol, J., & Samson, O. (2021). Body mass index and immune-related adverse events in patients on immune checkpoint inhibitor therapies: a systematic review and meta-analysis. *Cancer Immunol Immunother*, 70(1), 89-100. https://doi.org/10.1007/s00262-020-02663-z.

[Higashi et al., 2022] Higashi, Y., Ma, Y., Matsumoto, K., Shiro, A., Saitoh, H., Kawachi, T., & Tamanoi, F. (2022). Auger electrons and DNA double-strand breaks studied by using iodine-containing chemicals. *The Enzymes*, 51, 101-115. https://doi.org/10.1016/bs.enz.2022.08.007.

[Hollern et al., 2019] Hollern, D.P., Xu, N., Mott, K.R., He, X., Carey-Ewend, K., Marron, D., Ford, J.B., Parker, J.S., Vincent, B.G., Serody, J.S., & Perou, C.M. (2019). Abstract GS1-05: Apobec3 induced mutagenesis sensitizes murine models of triple negative breast cancer to immunotherapy by activating B-cells and CD4+ T-cells. *General Session Abstracts.*

[Hommes et al., 2021] Hommes, J.W., Verheijden, R.J., Suijkerbuijk, K.P.M., and Hamann, D. (2021). Biomarkers of checkpoint inhibitor-induced immune-related adverse events—A comprehensive review. *Frontiers in Oncology*, 10, 585311. https://doi.org/10.3389/fonc.2020.585311. PMID: 33643899; PMCID: PMC7905347.

[Hosseini et al. 2020] Hosseini, A., Gharibi, T., Marofi, F., Babaloo, Z., and Baradaran, B. (2020). CTLA-4: From mechanism to autoimmune therapy. *International Immunopharmacology*, 80, 106221.

[Hu et al., 2023] Hu, W.T., Zhang, Q., Zhang, Z., He, X., Zhou, M., Guo, Y., and Wang, X. (2023). Eosinophil and IFN-γ associated with immune-related adverse events as prognostic markers in patients with non-small cell lung cancer treated with immunotherapy. *Frontiers in Immunology*, 14, 1112409.

https://doi.org/10.3389/fimmu.2023.1112409. PMID: 36949952; PMCID: PMC10025375.

[Illouz et al., 2023] Illouz, F., Drui, D., Caron, P., and Do Cao, C. (2023). Immune checkpoint inhibitor-induced thyroiditis: From pathophysiological mechanisms to clinical management. *Endocrine Reviews*, 44(1), 92-114. https://doi.org/10.1210/endrev/bnad002.

[Iwama et al. 2014] Iwama, S., De Remigis, A., Callahan, M.K., Slovin, S.F., Wolchok, J.D., and Caturegli, P. (2014). Pituitary expression of CTLA-4 mediates hypophysitis secondary to administration of CTLA-4 blocking antibody. *Science Translational Medicine*, 6(230), 230ra245. https://doi.org/10.1126/scitranslmed.3008002.

[Iwama et al. 2022] Iwama, S., et al. (2022). Immune checkpoint inhibitor-related thyroid dysfunction. *Best Practice & Research Clinical Endocrinology & Metabolism*, 36(3), 101660. https://doi.org/10.1016/j.beem.2022.101660.

[Iyer et al. 2018] Iyer, P.C., Cabanillas, M.E., Waguespack, S.G., Hu, M.I., Thosani, S., Lavis, V.R., Busaidy, N.L., Subudhi, S.K., Diab, A., and Dadu, R. (2018). Immune-related thyroiditis with immune checkpoint inhibitors. *Thyroid*, 28(10), 1243-1251. https://doi.org/10.1089/thy.2018.0116. PMID: 30132401; PMCID: PMC6157359.

[Karaviti et al. 2024] Karaviti, D., Kani, E.R., Karaviti, E., et al. (2024). Thyroid disorders induced by immune checkpoint inhibitors. *Endocrine*, 85, 67–79. https://doi.org/10.1007/s12020-024-03718-2.

[Kassi et al. 2019] Kassi, E., Angelousi, A., Asonitis, N., Diamantopoulos, P., Anastasopoulou, A., Papaxoinis, G., Kokkinos, M., Giovanopoulos, I., Kyriakakis, G., Petychaki, F., Savelli, A., Benopoulou, O., and Gogas, H. (2019). Endocrine-related adverse events associated with immune-checkpoint inhibitors in patients with melanoma. *Cancer Medicine*, 8(15), 6585-6594. https://doi.org/10.1002/cam4.2533. Epub 2019 Sep 13. PMID: 31518074; PMCID: PMC6825974.

[Kaufman et al. 2016] Kaufman, H.L., Russell, J., Hamid, O., Bhatia, S., Terheyden, P., D'Angelo, S.P., Shih, K.C., Lebbé, C., Linette, G.P., Milella, M., Brownell, I., Lewis, K.D., Lorch, J.H., Chin, K., Mahnke, L., von Heydebreck, A., Cuillerot, J.M., and Nghiem, P. (2016). Avelumab in patients with chemotherapy-refractory metastatic Merkel cell carcinoma: A multicentre, single-group, open-label, phase 2 trial. *Lancet Oncol*, 17(10), 1374-1385. https://doi.org/10.1016/S1470-2045(16)30364-3. Epub 2016 Sep 1. PMID: 27592805; PMCID: PMC5587154.

[Kaur and Dufour, 2012] Kaur, G., and Dufour, J.M. (2012). Cell lines: Valuable tools or useless artifacts. *Spermatogenesis*, 2(1), 1-5. https://doi.org/10.4161/spmg.19885. PMID: 22553484; PMCID: PMC3341241.

[Keller et al., 2020] Keller, F., Bruch, R., Schneider, R., Meier-Hubberten, J., Hafner, M., and Rudolf, R. (2020). A scaffold-free 3-D co-culture mimics the major features of the reverse Warburg effect in vitro. *Cells*, 9(8), 1900. https://doi.org/10.3390/cells9081900. PMID: 32823793; PMCID: PMC7463893.

[Kijanska and Kelm, 2016] Kijanska, M., & Kelm, J. (2016). In vitro 3D Spheroids and Microtissues: ATP-based Cell Viability and Toxicity Assays. *Assay Guidance Manual [Internet].* Bethesda (MD): Eli Lilly & Company and the National Center for Advancing Translational Sciences. Available from: https://www.ncbi.nlm.nih.gov/books/NBK343426/.

[Kim et al. 2022] Kim, T.K., Vandsemb, E.N., Herbst, R.S., and Chen, L. (2022). Adaptive immune resistance at the tumour site: Mechanisms and therapeutic opportunities. *Nat Rev Drug Discov*, 21, 529–540.

[Kim et al., 2022] Kim, S.T., Chu, Y., Misoi, M., et al. (2022). Distinct molecular and immune hallmarks of inflammatory arthritis induced by immune checkpoint inhibitors for cancer therapy. *Nat Commun.*, 13(1), 1970. https://doi.org/10.1038/s41467-022-29539-3.

[Lechner et al., 2023] Lechner, M.G., Zhou, Z., Hoang, A.T., Huang, N., Ortega, J., Scott, L.N., Chen, H.C., Patel, A.Y., Yakhshi-Tafti, R., Kim, K., Hugo, W., Famini, P., Drakaki, A., Ribas, A., Angell, T.E., and Su, M.A. (2023). Clonally expanded,

thyrotoxic effector CD8+ T cells driven by IL-21 contribute to checkpoint inhibitor thyroiditis. *Science Translational Medicine*, 15(696), eadg0675. https://doi.org/10.1126/scitranslmed.adg0675. Epub 2023 May 17. PMID: 37196065; PMCID: PMC10227862.

[Lee et al., 2023] Lee, H.J., Manavalan, A., Stefan-Lifshitz, M., Schechter, C., Maity, A., & Tomer, Y. (2023). Permanent hypothyroidism following immune checkpoint inhibitors induced thyroiditis may be associated with improved survival: results of an exploratory study. *Front Endocrinol (Lausanne)*, 14, 1169173. https://doi.org/10.3389/fendo.2023.1169173.

[Lingel and Brunner-Weinzierl 2019] Lingel, H., and Brunner-Weinzierl, M.C. (2019). CTLA-4 (CD152): A versatile receptor for immune-based therapy. *Seminars in Immunology*, 42, 101298.

[Lipson and Drake, 2011] Lipson, E.J., and Drake, C.G. (2011). Ipilimumab: An anti-CTLA-4 antibody for metastatic melanoma. *Clinical Cancer Research*, 17(22), 6958–6962.

[Liu et al., 2022] Liu, R., Meng, X., Yu, X., Wang, G., Dong, Z., Zhou, Z., Qi, M., Yu, X., Ji, T., & Wang, F. (2022). From 2D to 3D Co-Culture Systems: A Review of Co-Culture Models to Study the Neural Cells Interaction. *Int. J. Mol. Sci.*, 23, 13116. https://doi.org/10.3390/ijms232113116.

[Lu et al. 2022] Lu, D., Yao, J., Yuan, G., Gao, Y., Zhang, J., and Guo, X. (2022). Immune checkpoint inhibitor-related new-onset thyroid dysfunction: A retrospective analysis using the US FDA adverse event reporting system. *The Oncologist*, 27(2), e126–e132. https://doi.org/10.1093/oncolo/oyab043.

[Meng et al. 2024] Meng, L., Wu, H., Wu, J., et al. (2024). Mechanisms of immune checkpoint inhibitors: Insights into the regulation of circular RNAs involved in cancer hallmarks. *Cell Death Dis*, 15, 3. https://doi.org/10.1038/s41419-023-06389-5.

[Migden et al. 2018] Migden, M.R., Rischin, D., Schmults, C.D., Guminski, A., Hauschild, A., Lewis, K.D., Chung, C.H., Hernandez-Aya, L., Lim, A.M., Chang, A.L.S., Rabinowits, G., Thai, A.A., Dunn, L.A., Hughes, B.G.M., Khushalani, N.I., Modi, B., Schadendorf, D., Gao, B., Seebach, F., Li, S., Li, J., Mathias, M., Booth, J., Mohan, K., Stankevich, E., Babiker, H.M., Brana, I., Gil-Martin, M., Homsi, J., Johnson, M.L., Moreno, V., Niu, J., Owonikoko, T.K., Papadopoulos, K.P., Yancopoulos, G.D., Lowy, I., and Fury, M.G. (2018). PD-1 Blockade with Cemiplimab in Advanced Cutaneous Squamous-Cell Carcinoma. *N Engl J Med*, 379(4), 341-351. https://doi.org/10.1056/NEJMoa1805131. PMID: 29863979.

[Mikoś et al., 2014] Mikoś, H., Mikoś, M., Obara-Moszyńska, M., & Niedziela, M. (2014). The role of the immune system and cytokines involved in the pathogenesis of autoimmune thyroid disease (AITD). *Endokrynol Pol*, 65(2), 150-155. https://doi.org/10.5603/EP.2014.0021.

[Nervo et al. 2023] Nervo, A., Ferrari, M., Gruosso, G., Migliore, E., Basile, S., D'Angelo, V., Roux, A., Piovesan, A., and Arvat, E. (2023). Immune-related thyroid dysfunctions during anti PD-1/PD-L1 inhibitors: New evidence from a single centre experience. *Clinical and Experimental Medicine*, 23(8), 4817-4824. https://doi.org/10.1007/s10238-023-01082-5. Epub 2023 Apr 27. PMID: 37103651.

[Oh et al., 2022] Oh, J.M., Gangadaran, P., Rajendran, R.L., Hong, C.M., Lee, J., & Ahn, B.-C. (2022). Different Expression of Thyroid-Specific Proteins in Thyroid Cancer Cells between 2-Dimensional (2D) and 3-Dimensional (3D) Culture Environment. *Cells*, 11, 3559. https://doi.org/10.3390/cells11223559.

[Olsson-Brown et al., 2020] Olsson-Brown, A., Lord, R., Sacco, J., Wagg, J., Coles, M., and Pirmohamed, M. (2020). Two distinct clinical patterns of checkpoint inhibitor-induced thyroid dysfunction. *Endocrine Connections*, 9(4), 318-325. Retrieved Jul 17, 2024, from https://doi.org/10.1530/EC-19-0473.

[Pampaloni et al., 2007] Pampaloni, F., Reynaud, E., and Stelzer, E. (2007). The third dimension bridges the gap between cell culture and live tissue. *Nature Reviews Molecular Cell Biology*, 8, 839–845. https://doi.org/10.1038/nrm2236.

[Pardoll, 2012] Pardoll, D. (2012). The blockade of immune checkpoints in cancer immunotherapy. *Nature Reviews Cancer*, 12, 252–264. https://doi.org/10.1038/nrc3239.

[Paschou et al., 2021] Paschou, S.A., Stefanaki, K., Psaltopoulou, T., Liontos, M., Koutsoukos, K., Zagouri, F., Lambrinoudaki, I., and Dimopoulos, M.A. (2021). How we treat endocrine complications of immune checkpoint inhibitors. *ESMO Open*, 6(1), 100011. https://doi.org/10.1016/j.esmoop.2020.100011. Epub 2021 Jan 4. PMID: 33399077; PMCID: PMC7807832.

[Patsoukis et al., 2020] Patsoukis, N., Wang, Q., Strauss, L., and Boussiotis, V.A. (2020). Revisiting the PD-1 pathway. *Science Advances*, 6, eabd2712.

[Powles et al., 2018] Powles, T., Durán, I., van der Heijden, M.S., Loriot, Y., Vogelzang, N.J., De Giorgi, U., Oudard, S., Retz, M.M., Castellano, D., Bamias, A., Fléchon, A., Gravis, G., Hussain, S., Takano, T., Leng, N., Kadel, E.E. 3rd, Banchereau, R., Hegde, P.S., Mariathasan, S., Cui, N., Shen, X., Derleth, C.L., Green, M.C., and Ravaud, A. (2018). Atezolizumab versus chemotherapy in patients with platinum-treated locally advanced or metastatic urothelial carcinoma (IMvigor211): A multicentre, open-label, phase 3 randomised controlled trial. *Lancet*, 391(10122), 748-757. https://doi.org/10.1016/S0140-6736(17)33297-X. Epub 2017 Dec 18. Erratum in: *Lancet*, 2018 Oct 20;392(10156):1402. https://doi.org/10.1016/S0140-6736(18)32516-9. PMID: 29268948.

[Powles et al., 2020] Powles, T., Park, S.H., Voog, E., Caserta, C., Valderrama, B.P., Gurney, H., Kalofonos, H., Radulović, S., Demey, W., Ullén, A., Loriot, Y., Sridhar, S.S., Tsuchiya, N., Kopyltsov, E., Sternberg, C.N., Bellmunt, J., Aragon-Ching, J.B., Petrylak, D.P., Laliberte, R., Wang, J., Huang, B., Davis, C., Fowst, C., Costa, N., Blake-Haskins, J.A., di Pietro, A., and Grivas, P. (2020). Avelumab Maintenance Therapy for Advanced or Metastatic Urothelial Carcinoma. *N Engl J Med*, 383(13), 1218-1230. https://doi.org/10.1056/NEJMoa2002788. Epub 2020 Sep 18. PMID: 32945632.

[Powles et al., 2020] Powles, T., van der Heijden, M.S., Castellano, D., Galsky, M.D., Loriot, Y., Petrylak, D.P., Ogawa, O., Park, S.H., Lee, J.L., De Giorgi, U., Bögemann, M., Bamias, A., Eigl, B.J., Gurney, H., Mukherjee, S.D., Fradet, Y., Skoneczna, I., Tsiatas, M., Novikov, A., Suárez, C., Fay, A.P., Duran, I., Necchi, A., Wildsmith, S., He, P., Angra, N., Gupta, A.K., Levin, W., and Bellmunt, J.; DANUBE study investigators. (2020). Durvalumab alone and durvalumab plus tremelimumab versus chemotherapy in previously untreated patients with unresectable, locally advanced or metastatic urothelial carcinoma (DANUBE): A randomised, open-label, multicentre, phase 3 trial. *Lancet Oncol*, 21(12), 1574-1588. https://doi.org/10.1016/S1470-2045(20)30541-6. Epub 2020 Sep 21. Erratum in: *Lancet Oncol*, 2021 Jan;22(1).

[Rahman and Bordoni, 2023] Rahman, M., and Bordoni, B. (2023). Histology, natural killer cells. In: StatPearls [Internet]. Treasure Island (FL): StatPearls Publishing; 2024 Jan-. Available from: https://www.ncbi.nlm.nih.gov/books/NBK565844/.

[Reck et al., 2016] Reck, M., Rodríguez-Abreu, D., Robinson, A.G., Hui, R., Csőszi, T., Fülöp, A., Gottfried, M., Peled, N., Tafreshi, A., Cuffe, S., O'Brien, M., Rao, S., Hotta, K., Leiby, M.A., Lubiniecki, G.M., Shentu, Y., Rangwala, R., and Brahmer, J.R. (2016). Pembrolizumab versus Chemotherapy for PD-L1-Positive Non-Small-Cell Lung Cancer. *N Engl J Med*, 375(19), 1823-1833. https://doi.org/10.1056/NEJMoa1606774. PMID: 27718847.

[Rittmeyer et al., 2017] Rittmeyer, A., Barlesi, F., Waterkamp, D., Park, K., Ciardiello, F., von Pawel, J., Gadgeel, S.M., Hida, T., Kowalski, D.M., Dols, M.C., Cortinovis, D.L., Leach, J., Polikoff, J., Barrios, C., Kabbinavar, F., Frontera, O.A., De Marinis, F., Turna, H., Lee, J.S., Ballinger, M., Kowanetz, M., He, P., Chen, D.S., Sandler, A., and Gandara, D.R. (2017). Atezolizumab versus docetaxel in patients with previously treated non-small-cell lung cancer (OAK): A phase 3, open-label, multicentre randomised controlled trial. *Lancet*, 389(10066), 255-265. https://doi.org/10.1016/S0140-6736(16)32517-X. Erratum in: *Lancet*, 2017 Apr 8;389(10077).

[Robert et al., 2019] Robert, C., Ribas, A., Schachter, J., Arance, A., Grob, J.J., Mortier, L., Daud, A., Carlino, M.S., McNeil, C.M., Lotem, M., Larkin, J.M.G., Lorigan, P., Neyns, B., Blank, C.U., Petrella, T.M., Hamid, O., Su, S.C., Krepler, C., Ibrahim, N., and Long, G.V. (2019). Pembrolizumab versus ipilimumab in advanced melanoma (KEYNOTE-006): post-hoc 5-year results from an open-label, multicentre, randomised, controlled, phase 3 study. *Lancet Oncol*, 20(9), 1239-1251. https://doi.org/10.1016/S1470-2045(19)30388-2. PMID: 31345627.

[Romano et al., 2015] Romano, E., Kusio-Kobialka, M., Foukas, P.G., Baumgaertner, P., Meyer, C., Ballabeni, P., et al. (2015). Ipilimumab-dependent cell-mediated cytotoxicity of regulatory T cells ex vivo by nonclassical monocytes in melanoma patients. *Proceedings of the National Academy of Sciences of the United States of America (PNAS)*, 112(19), 6140–6145. https://doi.org/10.1073/pnas.1417320112.

[Saraiva et al., 2020] Saraiva, D.P., Matias, A.T., Braga, S., Jacinto, A., & Cabral, M.G. (2020). Establishment of a 3D Co-culture With MDA-MB-231 Breast Cancer Cell Line and Patient-Derived Immune Cells for Application in the Development of Immunotherapies. *Front Oncol.*, 10, 1543. https://doi.org/10.3389/fonc.2020.01543.

[Shen et al., 2018] Shen, J., Xiao, Z., Zhao, Q., Li, M., Wu, X., Zhang, L., Hu, W., and Cho, C.H. (2018). Anti-cancer therapy with TNFα and IFNγ: A comprehensive review. *Cell Proliferation*, 51(4), e12441. https://doi.org/10.1111/cpr.12441. Epub 2018 Feb 26. PMID: 29484738; PMCID: PMC6528874.

[Singh et al., 2023] Singh, N., Hocking, A.M., and Buckner, J.H. (2023). Immune-related adverse events after immune checkpoint inhibitors: Understanding the intersection with autoimmunity. *Immunological Reviews*, 318, 81-88.

[Stelmachowska-Banaś and Czajka-Oraniec 2020] Stelmachowska-Banaś, M., and Czajka-Oraniec, I. (2020). Management of endocrine immune-related adverse events of immune checkpoint inhibitors: An updated review. *Endocrine Connections*, 9(10), R207-R228. Retrieved Jul 16, 2024, from https://doi.org/10.1530/EC-20-0342.

[Su et al., 2024] Su, J., Fu, Y., Cui, Z., Abidin, Z., Yuan, J., Zhang, X., Li, R., and Zhao, C. (2024). Relatlimab: A novel drug targeting immune checkpoint LAG-3 in melanoma therapy. *Front Pharmacol*, 14, 1349081. https://doi.org/10.3389/fphar.2023.1349081. PMID: 38269271; PMCID: PMC10806167.

[Taylor et al., 2023] Taylor, J., Gandhi, A., Gray, E., and Zaenker, P. (2023). Checkpoint inhibitor immune-related adverse events: A focused review on autoantibodies and B cells as biomarkers, advancements and future possibilities. *Frontiers in Immunology*, 13, 991433. https://doi.org/10.3389/fimmu.2022.991433. PMID: 36713389; PMCID: PMC9874109.

[Tembhare et al., 2022] Tembhare, P.R., Chatterjee, G., Chaturvedi, A., Dasgupta, N., Khanka, T., Verma, S., Ghogale, S.G., Deshpande, N., Girase, K., Sengar, M., Bagal, B., Jain, H., Shetty, D., Rajpal, S., Patkar, N., Agrawal, T., Epari, S., Shet, T., Subramanian, P.G., and Gujral, S. (2022). Critical role of flow cytometric immunophenotyping in the diagnosis, subtyping, and staging of T-cell/NK-cell non-Hodgkin's lymphoma in real-world practice: A study of 232 cases from a tertiary cancer center in India. *Frontiers in Oncology*, 12, 779230. https://doi.org/10.3389/fonc.2022.779230. PMID: 35299754; PMCID: PMC8923658.

[Twomey and Zhang, 2021] Twomey, J.D., and Zhang, B. (2021). Cancer immunotherapy update: FDA-approved checkpoint inhibitors and companion diagnostics. *AAPS J*, 23, 39. https://doi.org/10.1208/s12248-021-00574-0.

[van Akkooi, 2024] van Akkooi, A.C.J. (2024). Relatlimab, an immune checkpoint inhibitor that blocks LAG-3, the latest drug to be added to the arsenal of systemic therapies for melanoma: What does a surgical oncologist need to know? *Ann Surg Oncol*, 31, 1–3. https://doi.org/10.1245/s10434-023-14416-0.

[von Itzstein et al., 2022] von Itzstein, M.S., Gonugunta, A.S., Wang, Y., Sheffield, T., Lu, R., Ali, S., Fattah, F.J., Xie, D., Cai, J., Xie, Y., & Gerber, D.E. (2022). Divergent prognostic effects of pre-existing and treatment-emergent thyroid

dysfunction in patients treated with immune checkpoint inhibitors. *Cancer Immunol Immunother*, 71(9), 2169-2181. https://doi.org/10.1007/s00262-022-03151-2.

[Voskoboinik et al., 2015] Voskoboinik, I., Whisstock, J., and Trapani, J. (2015). Perforin and granzymes: function, dysfunction and human pathology. *Nature Reviews Immunology*, 15, 388–400. https://doi.org/10.1038/nri3839.

[Wang et al., 2023] Wang, S.J., Dougan, S.K., and Dougan, M. (2023). Immune mechanisms of toxicity from checkpoint inhibitors. *Trends in Cancer*, 9(7), 543-553. https://doi.org/10.1016/j.trecan.2023.04.002. Epub 2023 Apr 27. PMID: 37117135; PMCID: PMC10330206.

[Ward and Thompson, 2012] Ward, P.S., & Thompson, C.B. (2012). Signaling in Control of Cell Growth and Metabolism. *Cold Spring Harb. Perspect. Biol.*, 4, a006783. https://doi.org/10.1101/cshperspect.a006783.

[Weber et al., 2015] Weber, J.S., D'Angelo, S.P., Minor, D., Hodi, F.S., Gutzmer, R., Neyns, B., Hoeller, C., Khushalani, N.I., Miller, W.H. Jr., Lao, C.D., Linette, G.P., Thomas, L., Lorigan, P., Grossmann, K.F., Hassel, J.C., Maio, M., Sznol, M., Ascierto, P.A., Mohr, P., Chmielowski, B., Bryce, A., Svane, I.M., Grob, J.J., Krackhardt, A.M., Horak, C., Lambert, A., Yang, A.S., and Larkin, J. (2015). Nivolumab versus chemotherapy in patients with advanced melanoma who progressed after anti-CTLA-4 treatment (CheckMate 037): A randomised, controlled, open-label, phase 3 trial. *Lancet Oncol*, 16(4), 375-384. https://doi.org/10.1016/S1470-2045(15)70076-8. PMID: 25795410.

[Wiersinga 2019] Wiersinga, W.M. (2019). Graves' disease: Can it be cured? *Endocrinology and Metabolism (Seoul)*, 34, 29–38. https://doi.org/10.3803/EnM.2019.34.1.29.

[Wright and Johnson, 2023] Wright, J.J., and Johnson, D.B. (2023). Approach to the patient with immune checkpoint inhibitor-associated endocrine dysfunction. *The Journal of Clinical Endocrinology & Metabolism*, 108(6), 1514–1525. https://doi.org/10.1210/clinem/dgac689.

[Xu et al., 2020] Xu, Y., Fu, Y., Zhu, B., Wang, J., and Zhang, B. (2020). Predictive biomarkers of immune checkpoint inhibitors-related toxicities. *Frontiers in Immunology*, 11, 2023. https://doi.org/10.3389/fimmu.2020.02023. PMID: 33123120; PMCID: PMC7572846.

[Yakavets et al., 2020] Yakavets, I., Francois, A., Benoit, A., et al. (2020). Advanced co-culture 3D breast cancer model for investigation of fibrosis induced by external stimuli: optimization study. *Sci Rep.*, 10, 21273. https://doi.org/10.1038/s41598-020-78087-7.

[Yamauchi et al., 2019] Yamauchi, I., Yasoda, A., Matsumoto, S., Sakamori, Y., Kim, Y.H., Nomura, M., Otsuka, A., Yamasaki, T., Saito, R., Kitamura, M., et al. (2019). Incidence, features, and prognosis of immune-related adverse events involving the thyroid gland induced by nivolumab. *PLoS ONE*, 14, e0216954. https://doi.org/10.1371/journal.pone.0216954.

[Zhan et al., 2021] Zhan, L., Feng, H.F., Liu, H.Q., Guo, L.T., Chen, C., Yao, X.L., and Sun, S.R. (2021). Immune checkpoint inhibitors-related thyroid dysfunction: Epidemiology, clinical presentation, possible pathogenesis, and management. *Front Endocrinol (Lausanne)*, 12, 649863. https://doi.org/10.3389/fendo.2021.649863. PMID: 34177799; PMCID: PMC8224170.